ImmunoTargets and Therapy

Dovepress
Taylor & Francis Group

Open Access Full Text Article

ORIGINAL RESEARCH

Ultrasound-Mediated Non-Specific Splenic Immunopotentiation to Elicit Broad-Spectrum Anti-Neoplastic Effects

Wei Dong[1–4], Guihu Wang[1–3], Senyang Li[1–3], Qian Wang[1–3], Wenjuan Li[3], Heyuan Liu[3], Yingxue Liang[3], Zhe Zhou[1,2,4], Xinrui He[2,4], Wenlei Guo[2,4], Jianing Yuan[2,4], Yichao Chai[1,4], Jing Geng[1–3], Zongfang Li[1–4]

[1]National and Local Joint Engineering Research Center of Biodiagnostics and Biotherapy, the Second Affiliated Hospital, Xi'an Jiaotong University, Xi'an, People's Republic of China; [2]Shaanxi Provincial Clinical Medical Research Center for Liver and Spleen Diseases, CHESS-Shaanxi Consortium, the Second Affiliated Hospital, Xi'an Jiaotong University, Xi'an, People's Republic of China; [3]Center for Tumor and Immunology, the Precision Medical Institute, Xi'an Jiaotong University, Xi'an, People's Republic of China; [4]Department of Geriatric General Surgery, the Second Affiliated Hospital, Xi'an Jiaotong University, Xi'an, People's Republic of China

Correspondence:Zongfang Li; Jing Geng, Email lzf2568@mail.xjtu.edu.cn; jgeng18@xjtu.edu.cn

ImmunoTargets and Therapy downloaded from https://www.dovepress.com/
For personal use only.

Background: Splenic immunomodulation triggered by ultrasound shows a significant anti-inflammatory effect against various inflammatory diseases, whose mechanism is mainly attributable to the activation of cholinergic anti-inflammatory pathway (CAP). However, the potential role and underlying mechanism of splenic ultrasound stimulation in cancer management have been rarely reported and superficially defined.

Methods: Following optimization of ultrasonic parameters, this study evaluated the anti-tumor efficacy of splenic sonication across multiple tumor models (eg, orthotopic H22 hepatocellular carcinoma (HCC), orthotopic Hepa1-6 HCC, and subcutaneous 4T1 breast cancer), and applied flow cytometry to quantify dynamic alterations in immune cell populations. Furthermore, in orthotopic H22 HCC models, this study employed fluorescence-activated cell sorting, RNA sequencing, splenic nerve blockade via absolute ethanol ablation, and in vitro Ca^{2+} flux assays to delineate the mechanisms underlying ultrasound-mediated splenic anti-tumor immunity.

Results: This study first assessed the therapeutic effect of focused ultrasound precisely targeting the spleen (FUS sti. spleen) on various tumors at specific ultrasonic doses. It fully demonstrated that FUS directly stimulated splenic immune cell proliferation and activation (especially NK and CD8 T cells) rather than CAP excitation to modulate splenic immune function. Particularly, NK cells are much more indispensable and important in responding to FUS stimulation for cancer suppression than CD8 T cells. RNA sequencing of NK and CD8 T cells, as well as in vitro experiments revealed that FUS firstly regulated calcium-related signaling pathways to further modulate others, such as PI3K-AKT, Rap1, and Hippo pathways to promote immune cell proliferation, migration and activation to suppress cancer cell deterioration. Particularly, FUS sti. spleen and FUS intervention on the tumor synergistically induced the best tumor suppression than each of the two taken individually.

Conclusion: FUS sti. spleen facilitated immunocyte proliferation and activation through altering calcium-dependent signaling rather than CAP excitation to modulate anti-tumor immunity, indicating substantial clinical translation potential.

Keywords: focused ultrasound, spleen, FUS sti. spleen, splenic immunomodulation, tumor suppression

Introduction

The spleen is the largest secondary lymphoid organ, and an extensive meshwork of nerve fibers is distributed throughout the splenic compartments including the splenic nodules, periarteriolar lymphoid sheath, marginal zones, trabeculae, white pulp and red pulp.[1,2] Even more striking, the nerve fibers are co-localized with various subsets of dendritic cells (DCs), macrophages (Mφ), and lymphocytes (ie B cells and T cells).[2,3] As early as 30 years ago, some studies demonstrated that sympathetic nerve terminals in the spleen secrete norepinephrine (NE) interacting with T cells in response to stimulation, while the content of splenic norepinephrine significantly decreases following chemical or surgical sympathectomy.[4,5] It

Received: 12 May 2025
Accepted: 9 August 2025
Published: 24 August 2025

© 2025 Dong et al. This work is published and licensed by Dove Medical Press Limited. The full terms of this license are available at https://www.dovepress.com/terms.php and incorporate the Creative Commons Attribution – Non Commercial (unported, v4.0) License (http://creativecommons.org/licenses/by-nc/4.0/). By accessing the work you hereby accept the Terms. Non-commercial uses of the work are permitted without any further permission from Dove Medical Press Limited, provided the work is properly attributed. For permission for commercial use of this work, please see paragraphs 4.2 and 5 of our Terms (https://www.dovepress.com/terms.php).

Graphical Abstract

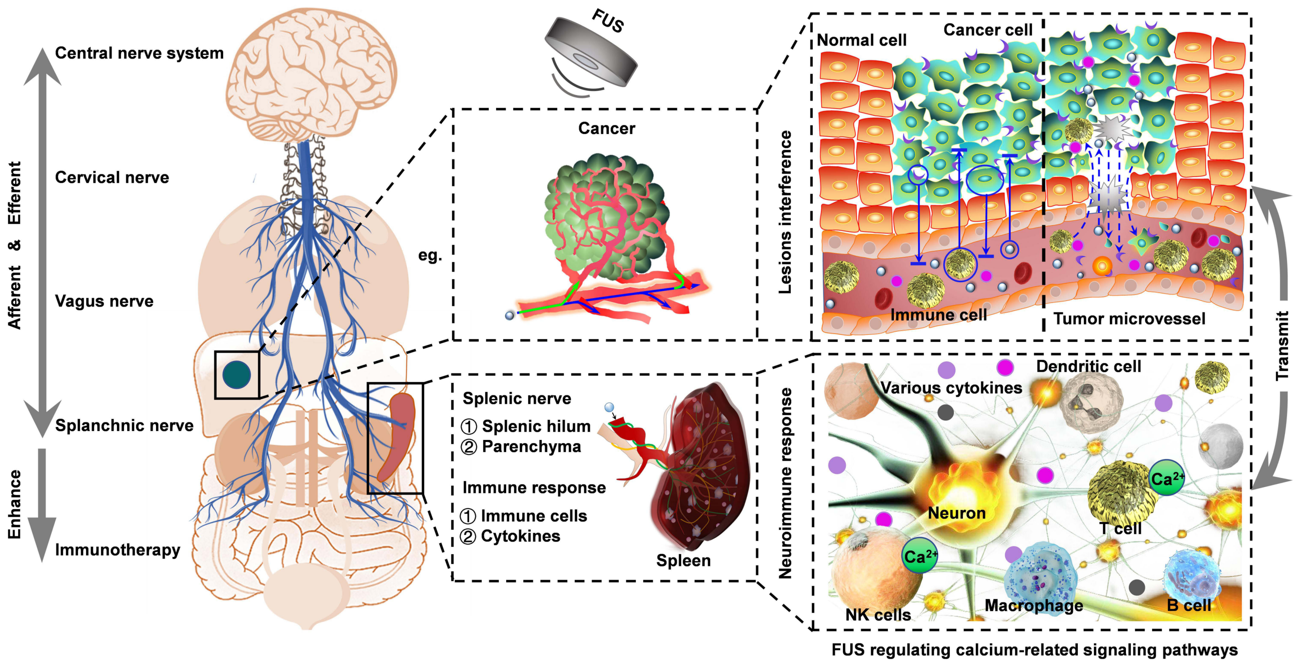

was not until around 2000 that the cholinergic anti-inflammatory pathway (CAP) concept was formally proposed and extensively studied because of its vital function in modulating the mammalian immune response.[6–10] The CAP mechanism relies on the parasympathetic vagus nerve transmitting signals from the brain to the adrenergic splenic nerve that interacts with immune cells (Supplementary Figure 1). Munyaka et al[11] revealed that CAP is activated after central cholinergic activation by intracerebroventricular infusion of the M1 muscarinic acetylcholine (ACh) receptor agonist in mice but is suppressed by vagotomy or splenic neurectomy. Moreover, Ji et al[12] proved that central cholinergic activation induced by the acetylcholinesterase inhibitor galantamine or the muscarinic ACh receptor agonist relieves colitis in mice, which is inhibited after vagotomy, splenic neurectomy or splenectomy. These reports indicate that spleen is a vital target of the CAP.

In the past decade, many researchers applied physical methods to trigger the splenic neural-immune reflex for regulating the immune response to chronic inflammatory diseases.[13] Inoue et al[14] utilized a bipolar silver wire electrode stimulating the isolated left cervical vagus nerve to attenuate kidney ischemia-reperfusion injury (IRI), suggesting that vagus nerve stimulation (VNS)-mediated IRI treatment and systemic inflammation depend on α7 nicotinic acetylcholine receptors (α7nAChR)-positive splenocytes. Koopman et al[15,16] reported that stimulation of the CAP by VNS to treat rheumatoid arthritis (RA) in experimental models and clinical trials exerts a significant mitigation effect, whilst the symptoms aggravated following unilateral cervical vagotomy or α7nAChR knockout in mice. Besides, Meregnani et al[17] demonstrated that the symptoms of colonic colitis in rats induced by trinitrobenzene sulphonic acid was significantly reduced after VNS performed with electrode cuffs for 5 days. Moreover, electroacupuncture intervention eliciting splenic efferent vagus nerve activity not only reduced tumor proliferation in breast tumor-bearing mice by alleviating inflammation and enhancing antitumor immunity,[18] but also could alleviate the severity of chemotherapy-induced nausea and vomiting in patients with advanced cancer.[19,20] In addition, bioelectronic devices for VNS in clinical application have already been approved by the European Medicines Agency and the US Food and Drug Administration (FDA) for the treatment of drug-refractory epilepsy and depression.[13,21,22]

Unsatisfactorily, nerve stimulation using permanently implanted electrodes, transcutaneous bioelectronic devices, or slightly injurious electroacupuncture was limited to stimulate large nerves or superficial nerves.[23] Peripheral organs, not just the spleen, are extensively traversed by peripheral nervous system, which makes it difficult to selectively stimulate subsets of axons that terminate in spleen and uniquely modulate the immune response to inflammatory diseases.[23] For example, cervical nerve stimulation usually activates the extensive efferent and afferent neural pathways that elicit neural responses from non-target organs.[13,16,24–26] Although scientists are committed to developing more advanced, miniaturized and sophisticated electrode designs for implantation on specific nerves near the target organ,[27,28] invasive implantation easily causes damage to the delicate nerve fibers of the target organ and it is difficult to stimulate nerves throughout the organ. Thus, new nonintrusive strategies are imperative to trigger specific nerves, especially the splenic nerve, and mobilize the splenic immune function against diseases.

Notably, recent studies showed that noninvasive ultrasound successfully elicits peripheral nerve activation in the spleen to treat chronic inflammatory diseases (Supplementary Figure 1). Gigliotti JC and co-workers[29] used an ultrasound imaging probe to successfully irradiate the neural innervation in the spleen mitigating IRI in mice, whose mechanism is mainly attributable to the CAP activation.[6,9,16,24] Later, Cotero et al[23] reported that ultrasound modulating splenic nerve reduces endotoxin-induced cytokine production at a level comparable with traditional VNS performed with electrodes. Zachs et al[30] applied ultrasound stimulation targeting the spleen, which significantly reduces inflammation severity in RA mouse models. These studies provide ample evidence on the potential of precise splenic ultrasound stimulation to replace bioelectronic devices for the translation of peripheral neuromodulation-based therapies for inflammatory disease. However, the potential roles and underlying mechanisms of splenic ultrasound stimulation in cancer management have been rarely reported and superficially defined. Upon validation of its significant antitumor efficacy, splenic ultrasound stimulation would represent a groundbreaking clinical advancement by circumventing multiple limitations of conventional cancer therapies: surgical resection-associated recurrence and visceral injury compromising quality of life, chemotherapy-induced systemic toxicity, off-target risks of immunotherapy, and the technical complexities of personalized gene therapy.[31]

Further investigation is needed to establish whether ultrasound directly regulates the immunomodulatory function of the spleen by interfering with splenic immune cells and microenvironment. Ultrasound targeting the spleen is crucial in achieving conspicuously therapeutic effects, since the stimulation of other body locations or the lack of immune cells in mice is noneffective, which suggests the indispensability and importance of immune cells.[29,30] Cotero et al[23] and Zachs et al[30] concluded that ultrasound activating CAP indirectly exerts an influence on splenic immune cells or cytokines to reduce the severity of lipopolysaccharide acute inflammation and RA, but they mainly focused on the analysis of neuro-immune mechanism and did not perform a systematic research on the changes of splenic immune cells in response to ultrasonic stimulation. Generally, ultrasonic irradiation on cells directly irritates the expression of multiple key genes/signaling pathways or interferes with the secretion of cytokines to regulate cell proliferation, differentiation and migration, such as stimulating the expression of vascular endothelial growth factor in several cells including endothelial cells, neural cells and ischemic cells.[32–35] Therefore, we hypothesized that ultrasound could effectively immunomodulated on the splenic immune cells responding to cancer cell antigens in splenic microenvironment, and enhance the proliferation, activation, migration, and information dissemination of immune cells during cancer immunotherapy.

Accordingly, this study was designed to explore whether focused ultrasound precisely stimulating spleen (FUS sti. spleen) was effective in suppressing tumor proliferation, and the underlying mechanisms regulating splenic ultrasound stimulation in cancer management, including the activation of splenic nerve-related CAP, and splenic immune cells responding directly to ultrasonic capabilities. The therapeutic efficacy of FUS sti. spleen was first assessed on various tumors under specific parameters screened before. Furthermore, the splenic immunomodulation through FUS sti. spleen was evaluated based on the changes of splenic immune cell population and cytokine levels. Subsequently, nerve blockade, immune cell clearance and RNA sequencing were performed to identify the underlying mechanisms of splenic ultrasound stimulation in cancer management, such as splenic nerve-related CAP activation and FUS directly modulating immune cells, and the related molecular mechanism.

Methods

Cell Lines and Animal Models

Hepatocellular carcinoma (HCC) cell lines (H22 and hepa1-6) and 4T1 breast cancer cell line were purchased from the American Type Culture Collection (ATCC) and used for subsequent analysis. H22 cells were reproduced by ascites after intraperitoneal injection in C57black/6 mice (0.5–1.5*10^7 cells/mL; 200 µL per mouse). Hepa1-6 cells and 4T1 cells were cultured in Dulbecco's modified Eagle's medium (Cat. No. 11320033, Gibco, Invitrogen, Carlsbag, USA) supplemented with 10% fetal bovine serum (FBS; Cat. No. A5669701, Gibco, Invitrogen, Carlsbag, USA) and 1% penicillin-streptomycin solution (Cat. No. 15140122, Gibco, Invitrogen, Carlsbag, USA), and incubated at 37 °C under 5% CO_2 and 100% humidity.

Seven-week (weighted ~17 g) C57black/6 mice, purchased from the Beijing Animal Experiment Center (Chinese Academy of Sciences, Beijing, China), were housed at 24±2 °C under a 12-h light/dark cycle and acclimatized for at least 1 week before the experiments. All animals had access to sterilized food and water ad libitum. An amount of 0.2 mL H22 cancer cells (approximately 1–3*10^6 cells/mL) or 4T1 cancer cells (1–3*10^6 cells/mL) was hypodermically injected into the dorsal hindlimb region of the mouse to establish a subcutaneous tumor model. Regarding the in situ xenograft HCC models, an incision of approximately 1 cm in length was made at the upper end of the midabdominal line after the mouse was anesthetized with isohalothane and fixed on the anatomic stage. A total of 25 µL H22 cancer cells (approximately 0.5–1.5*10^7 cells/mL) or 50 µL hepa1-6 cancer cells (approximately 4–6*10^6 cells/mL) was injected into left hepatic lobe with an insulin syringe, and the incision was closed after applying pressure on the pinhole with a medical cotton swab for 3–4 minutes.

The tumor volume was calculated as follows: volume = 0.5*L*W^2, where L and W were the length and width of the tumor, respectively, measured by a caliper. The weight of spleen, tumor and mice was assessed by electronic scales. The splenic index was calculated by the ratio of spleen weight to mouse weight.

Ultrasonic Platform Set-up and Application for Spleen Stimulation

A diagram of the FUS system is shown in Supplementary Figure 2A. A function generator (Cat. No. 33120A, Agilent, Santa Clara, USA) produced a pulsed sinusoidal waveform triggering the power amplifier (Cat. No. AG1019, California, USA; or RPR-4000, RITEC Inc., Warwick, RI, USA) to drive a 1.04 MHz FUS transducer with a 100 mm aperture and 65 mm focus, whose focal region was ~1.4*1.4*8.6 mm^3 (Supplementary Figure 2B and C). The acoustic pressure and spatial beam profile of the FUS transducer were measured using a hydrophone (Cat. No. HNR-1000, ONDA, Videlles, France). The FUS transducer was mounted on a XYZ motorized positioning stage to control ultrasonic duration, and the position of the FUS focus relative to the mice was adjusted under a B-mode imaging guidance with a 3.2 MHz phased array positioned at the center of the FUS transducer.

The mice were anesthetized with 2–3% inhaled isoflurane and placed on a manual translation stage equipped with heating pad. Then, a centrifuged coupling gel was immediately applied to the shaved skin, and the manual translation stage was adjusted to allow the spleen (or tumor) site to be in tight contact with the bottom of the water tank under the B-mode imaging guidance (Supplementary Figure 2D). The FUS transducer was moved across the whole spleen (or tumor) through the XYZ programmable logical controller (Supplementary Figure 2E).

Flow Cytometry

Single-cell suspensions from the spleen, peripheral blood, tumor, and para-carcinoma tissue were obtained after red blood cells were lysed using lysis buffer (Cat. No. 555899, BD Bioscience, USA) according to the manufacturer's instructions. Cell suspensions were washed with sterilized PBS, and then incubated with the antibodies listed in Supplementary Table 1, and the scheme of antibody labeling for each immune cell is shown in Supplementary Table 2. Next, the immune cells were counted by flow cytometry (FCM) using CytoFLEX LX (Beckman Coulter Life Sciences, USA) after filtration through a 70-µm nylon cell strainer (Cat. No. 352350, Corning, USA). Data were analyzed using the FlowJo software (FlowJo 10, LLC, Ashland, OR).

Cytokine Measurement

Luminex Assay

Cytokine/chemokine quantification in plasma was performed by Luminex xMAP technology using a magnetic Luminex assay (R&D Systems, Minneapolis, MN, USA). The quantification was carried out using a Luminex® 200 Flow Cytometry System (Cat. No. x-200, Thermo Fisher Scientific, MA, USA) and Milliplex Analyst software (Version 5.1, Merck Millipore, MA, USA).

ELISA

The concentration of NE, ACh, granzyme and perforin in plasma, respectively, detected by enzyme-linked immunosorbent assay (ELISA). The operation processes were carried out in strict accordance with the instruction manual from Mouse Perforin ELISA Kit (Cat. No. F30718-A, FANKEW, Shanghai, China), Mouse Granzyme-B ELISA Kit (Cat. No. F3214-A, FANKEW, Shanghai, China), Mouse ACh ELISA Kit (Cat. No. MU30072, Bioswamp, Wuhan, China) and Mouse NE ELISA Kit (Cat. No. MU30372, Bioswamp, Wuhan, China), respectively.

Histological and Immunohistochemical Staining

Hematoxylin eosin (HE) staining was applied to evaluate the pathological changes of the spleen after FUS irradiation. Transferase-mediated deoxyuridine triphosphatebiotin nick end labeling (TUNEL) staining was performed to observe splenic cell apoptosis through the colorimetric TUNEL Apoptosis Assay Kit (Cat. No. C1091, Beyotime, Shanghai, China). The primary antibodies of anti-Ki67 (Cat. No. RM9106S1, Thermo Fisher Scientific, MA, USA; dilution 1:200), anti-NK1.1 (Cat. No. 108759, BioLegend, California, USA), anti-CD8a (Cat. No. ab4055, Abcam, Cambridge, UK; dilution 1:1000), and anti-c-Fos (Cat. No. ab222699, Abcam, Cambridge, UK; dilution 1:2000) were used for immunohistochemical staining to detect the protein expression of cyclin-D1, Ki67, NK1.1, CD8a, and c-Fos respectively. At least 5–10 different regions in each section were randomly selected for image acquisition using a fluorescence microscopy (observer3, Carl Zeiss, Jena, Germany), and the positive area ratio was quantified using the Image Pro Plus 6.0 software (Media Cybernetics, CA, United States).

RNA Sequencing

Approximately $1*10^7$ CD8 T cells ($CD45^+$ $CD3^+$ $CD8a^+$) and $5*10^6$ NK cells ($CD45^+$ $CD3^-$ $NK1.1^+$) were sorted from the spleen using the Beckman Kurt MoFlo Astrios ultra high-speed flow cytometry sorting system (MoFlo Astrios EQ, Beckman Coulter, lnc, USA). Subsequently, general transcriptome sequencing was performed when the positive cell rate was greater than 90% detected by flow cytometry (CytoFLEX LX, Beckman Coulter Life Sciences, USA). The cDNA library construction and sequencing of all RNA samples were performed by Shanghai OE Biotech Co., LTD. Transcriptome sequencing was performed to screen differentially expressed genes (DEGs). Then, gene ontology (GO) and Kyoto Encyclopedia of Genes and Genomes (KEGG) pathway enrichment analysis were applied to annotate the function of the DEGs. The DEG screening criteria were as follows: $P < 0.05$ and differential fold change $|\text{logFC}| \geq 1$.

Nerve Signal Blockade

Propranolol Hydrochloride Blocking CAP

Propranolol hydrochloride (Cat. No. abs44129405, Absin, Shanghai, China), a kind of adrenergic receptor antagonist, was intraperitoneally administered at a dose of 3 mg/kg to block CAP by directly binding to the adrenergic receptor at 1.5 hours before FUS exposure to spleen according to previous reports,[36–38] which ensured FUS sti. spleen at the optimal time point of CAP blockade.

Absolute Ethanol-Induced Splenic Nerve Block

Absolute ethanol was used for splenic nerve block according to previous studies.[39–44] Briefly, the mice were anesthetized with the isoflurane, and disinfection with iodophor was performed on the shaved skin. A 7–10 mm incision was made next to the left side of the spleen. The spleen was isolated with tweezers to keep it away from the peritoneal cavity for a clear exposure of the three main blood supply vascular trees. A wet cotton was used to protect the peritoneal cavity and other organs. Subsequently, absolute ethanol was repeatedly applied to those vascular trees with a cotton tip for 5–10 seconds each time, with an interval of five seconds, for a total of seven times to block the splenic nerve fibers. Excessive ethanol dripping from the cotton tip was carefully avoided, to avoid significant vasospasm, which could lead to permanent damage to blood vessels, consequently leading to spleen necrosis and organ complete absorption. As regards the sham-operated mice, the same entire surgical procedure was performed except for the repeated application of anhydrous ethanol that was replaced by normal saline (pH = 7.4).

In vivo Immune Cell Depletion

The experimental C57BL/6 mice were treated with an intravenous injection of Ultra-LEAF™ purified anti-mouse NK1.1 antibody (Cat. No. 108759, BioLegend, California, USA) or Ultra-LEAF™ purified anti-mouse CD8a antibody (Cat. No. 100763, BioLegend, California, USA) at a dose of 50 μg/mouse on day 0, 3, 7, 12 and 17 to deplete NK cell or CD8 T cell. As regards MDSC depletion, the Ultra-LEAF™ Purified anti-mouse Ly-6G antibody (Cat. No. 127650; BioLegend, California, USA) was intraperitoneally administered to C57BL/6 mice at a dose of 0.25 mg/mouse on day 0, 6, 12, and 18. The cell clearance efficacy was assessed by FCM.

Calcium Detection and in vitro Anticancer Experiment of FUS Stimulating Splenic CD8 T Cells or NK Cells Enhanced by Calcium

Von Kossa Staining

The splenic specimens were cut into 5 μm-thick sections and subjected to VON KOSSA Calcium Staining Kit (Cat. No. JM1519; HPBIO, Shanghai, China) for the histological visualization of calcium deposits (mineralization). Calcium deposition in splenic cells was assessed by fluorescence microscopy (Zeiss observer3), where mass deposits appeared black, while dispersed deposits appeared gray. The positive area ratio was quantified using the Image Pro Plus 6.0 software.

FCM Detection of Fluo-4 AM Labeled Cells

The splenic cell suspensions were washed twice with sterilized PBS, and then incubated with Fluo-4 AM dye (1 mL dye/ 10^6 cells; Cat. No. S1061M, Beyotime, Shanghai, China) for 30 min at 37 °C according to the manufacturer's instructions. Next, the fluorescent cells were monitored by FCM using the CytoFLEX LX (Ex/Em = 490/525 nm).

In vitro Experiments Verifying Calcium-Strengthened FUS Stimulating Splenic NK Cells Against Tumor

Approximately $1.2*10^6$ NK cells were sorted from the spleen using the Beckman Kurt MoFlo Astrios ultra high-speed flow cytometry sorting system, and then subjected to FUS stimulation with or without high calcium concentration (300 nM). Then, NK cells were co-cultured with pEGFP-C1 plasmid-transfected Hepa1-6 cancer cells at a ratio of 1:1, where GFP fluorescent protein was used to distinguish cancer cells from splenic cells. Transwell devices (Corning Incorporated, NY, USA) with 3-μm diameter holes were used to distinguish immune cells in the superstratum and cancer cells in the substratum. The cells were co-cultured for 48 h before GFP fluorescence observation with the Zeiss observer3, CCK-8 assay (Cat. No. ABS50003-500T, Univ, China), and crystal violet (CV) staining to assess cancer cell suppression and immune cell proliferation. The tumoral background was mimicked by adding ultrasound shattered cancer cell suspension to the NK cells solution during FUS stimulation.

Statistical Analysis

Statistical analysis was performed using the statistical product and service solutions software (SPSS, USA). Statistical significance was analyzed using Student's *t*-test for parametric data and Mann–Whitney *U*-test for nonparametric comparisons, with Bonferroni correction (specially for multiple comparisons), and the results were expressed as mean ± SEM. A value of $p < 0.05$ was considered statistically significant (*p < 0.05, **p < 0.01, and ***p < 0.001).

Results

Screening and Optimization of Ultrasonic Parameters for Spleen Stimulation

In view of the different ultrasonic parameters and platforms applied in previous studies of splenic ultrasound stimulation, it is pseudoscientific to indiscriminately imitate their ultrasonic parameters or methods to this study for regulating splenic immunotherapy to anti-cancer. Based on the pre-experiment results, 11 processing groups were set-up: G1-G11 group (detailed in Table 1), for the screening and optimization of ultrasonic parameters, and FUS sti. spleen in subsequent experiments was performed once every other day starting from the 2nd day after cancer cell implantation, with a total experimental duration of 28 days (Figure 1A). At the experimental endpoint (day 29), animals underwent terminal anesthesia followed by comprehensive tissue harvesting for other experimental analyses (eg, HE and TUNEL staining). The degree of subcutaneous H22 tumor suppression and spleen injury (assessed by HE and TUNEL staining) was used as the decisive criterion to establish the appropriate ultrasonic parameters.

The phenotypic results showed that FUS sti. spleen significantly suppressed the proliferation of subcutaneous H22 tumor, especially in the G4, G5, G8 and G11 group (Figure 1B–D). The weight of the mice subjected to FUS sti. spleen was lower than that of the non-FUS mice (Figure 1E), and FUS sti. spleen showed a tendency to decrease splenomegaly (Figure 1F and G). By comparison, the increase of the duty cycle or the FUS exposure time at 1.8 MPa did not improve the anti-tumor effect (G3, G6, G9 and G10 group; Figure 1B–D). However, the high peak negative pressure of 2.8 MPa induced a severe spleen injury, easily leading to the death of mice (G5 group; Figure 1B, H and I). In contrast, FUS sti. spleen effectively suppressed tumor proliferation without damaging the splenic cells at 2.3 MPa (Figure 1B–D, H and I). However, the antitumor effect was significantly reduced when the FUS exposure time of 20s was shortened to 10s (G4 and G7 group; Figure 1B–D). FUS damaged a few splenic cells once increasing the exposure time of 20s to 40s or the duty cycle of 1% to 10% (G4, G8 and G11 group; Figure 1B–D, H–I). The above splenic stimulation results demonstrated a clear "dose response" to ultrasound with a distinct power level required for the specific regulation of biophysical effects on splenic immune cells, which was similar to previous studies.[23,29,30] In conclusion, the ultrasonic parameters of the G4 group (2.3 MPa, 1%, 20s) were selected for subsequent experiments of splenic immunomodulation for cancer therapy.

FUS Universally Activated Spleen Immunological Function to Suppress the Proliferation of Various Tumors

FUS Activated Splenic Immune Cells to Suppress the Proliferation of the Xenograft HCC in situ

The mouse model of HCC in situ, which was better to resemble the situation of primary liver cancer, was used to assess the anticancer efficiency of FUS sti. spleen. The orthotopic HCC mice were subjected to FUS sti. spleen from day 0 after

Table 1 Scheme of Different Ultrasonic Parameters for FUS Sti. Spleen

Groups	Tumor	Ultrasonic Parameters		
		Peak Negative Pressure (MPa)	Duty Cycle (%)	Exposure Time (s)
G1	×	×	×	×
G2	√	×	×	×
G3	√	1.8	1	20
G4	√	2.3	1	20
G5	√	2.8	1	20
G6	√	1.8	1	40
G7	√	2.3	1	10
G8	√	2.3	1	40
G9	√	1.8	10	20
G10	√	1.8	20	20
G11	√	2.3	10	20

Notes: The checkmark (√) indicates presence/adoption, while crossmark (×) indicates absence/non-adoption. G1-G11, experimental groups.

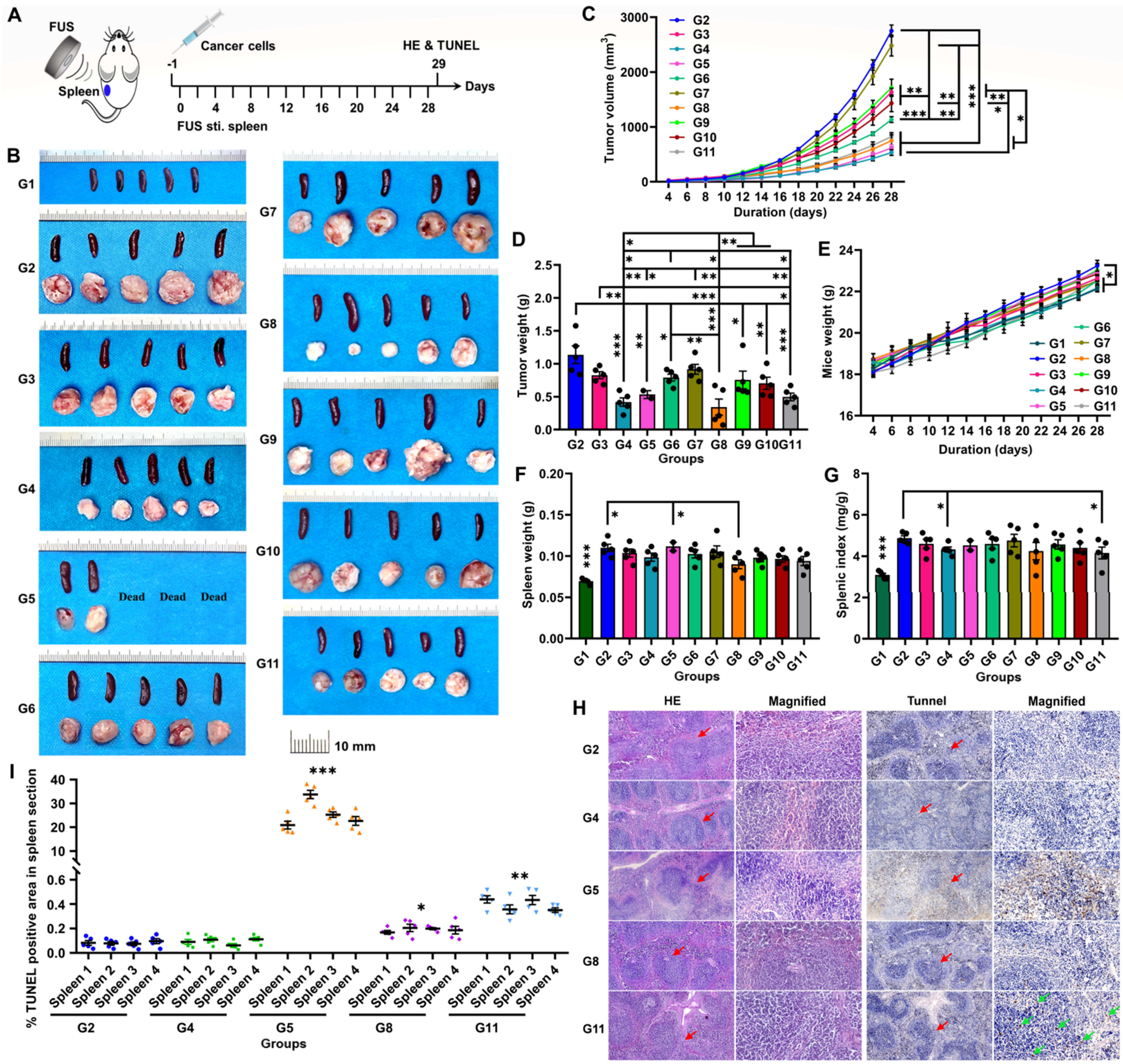

Figure 1 Inhibitory effect of FUS sti. spleen on subcutaneous H22 tumor under various ultrasonic parameters. (**A**) experimental flow diagram. (**B**) images of spleen and tumor in G1-G11 groups. (**C**) tumor growth curves. (**D**) tumor weight. (**E**) mice weight. (**F**) spleen weight. (**G**) spleen index. (**H**) HE and TUNEL staining of the spleen irradiated with FUS under different ultrasonic parameters; the red arrow indicates the area of the magnified image, and the green arrow indicates the TUNEL-positive cells. (**I**) analysis of TUNEL positive area. (n = 5; * p ≤ 0.05; **p ≤ 0.01; ***p ≤ 0.001; mean ± SEM). G1-G11 group details are shown in Table 1.

cancer cell implantation, and once every two days for a total experimental duration of 20 days (Figure 2A). At the experimental endpoint (day 21), animals underwent terminal anesthesia followed by comprehensive tissue harvesting for other experimental analyses (eg, FCM).

Twenty orthotopic H22 HCC mice were randomly divided into two groups: the S1 group was used as the control group, and the S2 group was subjected to FUS sti. spleen. The results of visual observation, tumor volume and tumor weight demonstrated that FUS sti. spleen significantly suppressed the proliferation of xenograft H22 carcinoma in situ, with a tumor inhibition rate of up to ~70% as compared with the control group (S2 vs S1, p<0.001; Figure 2B–D). Although the mean value of liver weight (total weight of the tumor and liver parenchyma) showed a decreasing trend in the S2 group compared to the S1 group, no significant difference was observed between the two groups (Figure 2E). In addition, the weight of the mice in the S2 group was lower than that of the mice in the S1 group (p<0.001; Figure 2F).

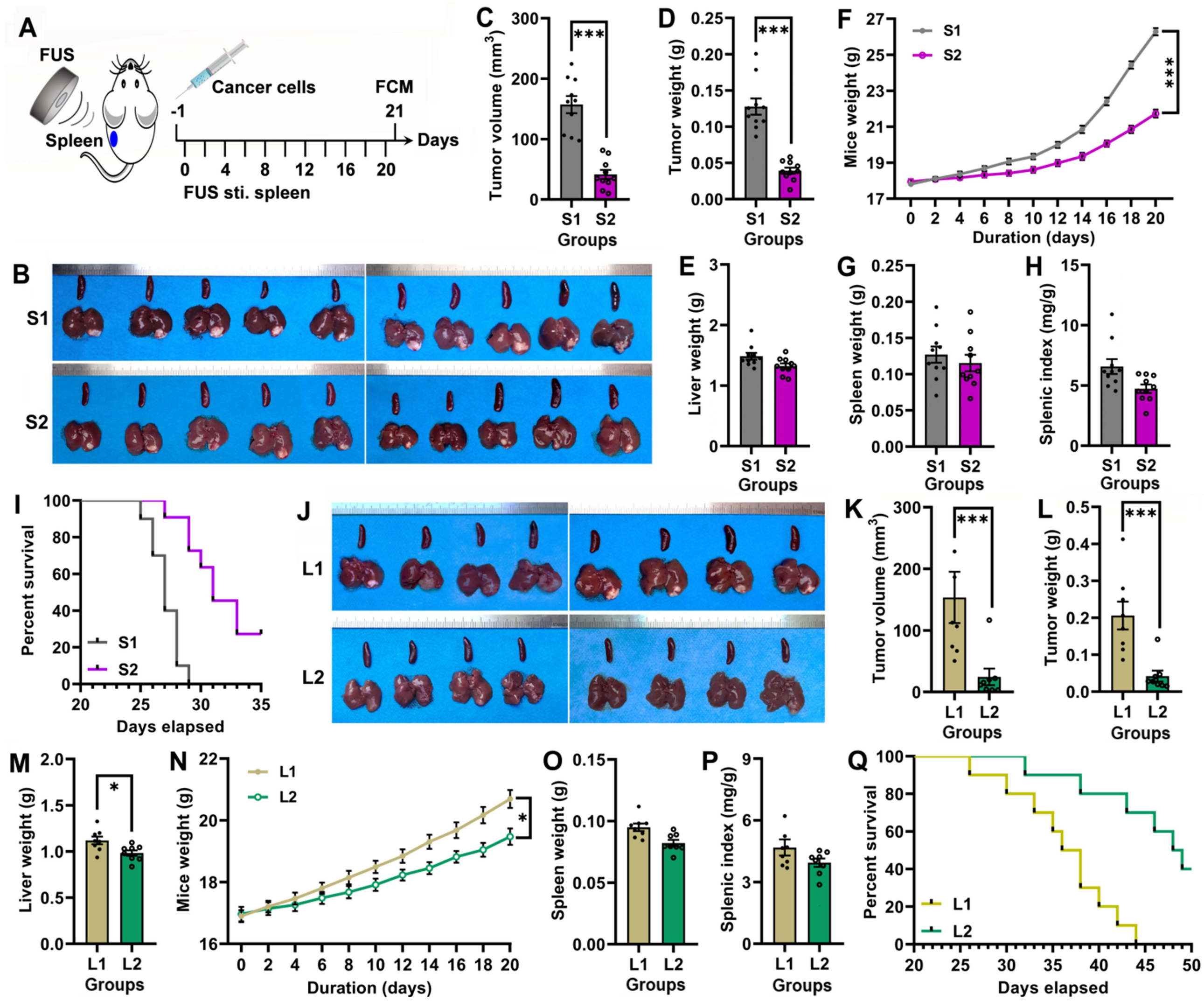

Figure 2 FUS sti. spleen suppressed the proliferation of the xenograft HCC in situ. (**A**) experimental flow diagram of FUS sti. spleen after HCC cancer cell implantation. (**B**–**I**) results of FUS sti. spleen suppressing the proliferation of the xenograft H22 HCC in situ. (**B**) images of spleen and xenograft H22 HCC in situ. (**C** and **D**) tumor volume and tumor weight, respectively. (**E**–**G**) liver weight, mice weight and spleen weight, respectively. (**H**) spleen index calculated by the ratio of spleen weight to mouse weight. (**I**) survival curves. S1, control group of xenograft H22 HCC in situ; S2, FUS sti. spleen started on day 0 after H22 cancer cell implantation. (**J**–**Q**) results of FUS sti. spleen suppressing the proliferation of the xenograft Hepa1-6 HCC in situ. (**J**) images of spleen and xenograft Hepa1-6 HCC in situ. (**K** and **L**), tumor volume and tumor weight, respectively. (**M**–**O**, liver weight, mice weight and spleen weight, respectively. (**P**) spleen index calculated by the ratio of spleen weight to mouse weight. (**Q**) survival curves. (n = 10; * p ≤ 0.05; ***p ≤ 0.001; mean ± SEM). L1, control group of xenograft Hepa1-6 HCC in situ; L2, FUS sti. spleen started on day 0 after Hepa1-6 cancer cell implantation.

The spleen weight and spleen index showed a decreasing trend of splenomegaly in the S2 group as compared with the S1 group, but without statistically significant difference (Figure 2G and H). More importantly, the survival statistics proved that the orthotopic H22 HCC mice treated with FUS sti. spleen had a longer survival time than the control group (Figure 2I).

Sixteen orthotopic Hepa1-6 HCC mice were randomly divided into two groups: L1 group was performed as the control group, and L2 group was administered to FUS sti. spleen. The results of visual observation, tumor volume and tumor weight showed that FUS sti. spleen remarkablely inhibited the proliferation of xenograft Hepa1-6 carcinoma in situ, with an antitumor ratio of up to ~80% (L2 vs L1, $p<0.001$; Figure 2J and L). Additionally, the weight of the liver and mice in the L2 group was lower than that of the mice in the L1 group ($p<0.05$; Figure 2M and N). No significant difference in spleen weight and spleen index was observed, although there was a decreasing trend shown in the L2 group as compared with the L1 group (Figure 2O and P). It was noteworthy that the survival time of the mice in the L2 group was significantly longer than that of the mice in the L1 group (Figure 2Q).

Thereafter, FCM results revealed that the proportion of tumor suppressor related immune cells in the spleen, blood, tumor and para-carcinoma tissue was significantly increased in the S2 group as compared with the S1 group, such as Th2 cells, NK cells, CD8 T cells, Mφ (Mφ2) and DC1 in the spleen; B cells, NK cells, CD8 T cells, Mφ1 and DC1 in the blood; CD4 T cells, NK cells, CD8 T cells, Mφ (Mφ1) and DC1 in the tumors; Th1 cells, NK cells, CD8 T cells and Mφ (Mφ1) in the para-carcinoma tissue (Table 2, Supplementary Figures 3–6). Moreover, the proportion of negative immune cells was significantly reduced, such as Treg cells and MDSCs (M-MDSCs and PMN-MDSCs) in both spleen and tumor; Th17, PMN-MDSCs in the blood; and PMN-MDSCs in the para-carcinoma tissue (Table 2, Supplementary Figures 3–6).

As regards to orthotopic Hepa1-6 HCC mice, FCM results showed that the number of positive anticancer immune cells in the spleen, blood, tumor and para-carcinoma tissue was significantly increased in the L2 group than in the L1 group, such as Th2 cells, NK cells, CD8 T cells, Mφ and DCs in the spleen; CD4 T cells, Th2 cells, NK cells, CD8 T cells, Mφ1, Mφ2 and DCs in the blood; NK cells, CD8 T cells, Mφ and DCs in the tumor; and NK cells, CD8 T cells and Mφ (Mφ1 and Mφ2) in the para-carcinoma tissue (Table 2, Supplementary Figures 7–10). The number of negative immune cells was significantly reduced, such as Treg cells and PMN-MDSCs in the spleen; Th17 and MDSCs in the blood; Th17 and PMN-MDSCs in the tumor; and PMN-MDSC in the para-carcinoma tissue (Table 2, Supplementary Figures 7–10).

These results fully demonstrated the significant effect of FUS on splenic immunomodulation for cancer immunotherapy. Particularly, FUS sti. spleen remarkably increased the proportion of NK cells and CD8 T cells in the spleen, blood, tumor and para-carcinoma tissue, followed by Mφ and DCs, whilst it reduced the number of PMN-MDSCs in all tissues with one accord, and then Treg cells.

Additionally, we assessed the therapeutic efficacy of FUS sti. spleen on subcutaneous 4T1 breast tumor, and further quantitatively evaluated the alterations in immune cell proportions following FUS intervention. Obviously, FUS sti. spleen demonstrated potent antitumor efficacy, achieving 70% tumor growth inhibition and significantly prolonging survival. FCM revealed that FUS elicited significant immunomodulatory effects, particularly enhancing NK cell and CD8+ T cell populations while suppressing immunosuppressive cells. The complete results are available in Supplementary File 1.

FUS Sti. Spleen Altered the Cytokine Levels

In addition to the modulation of cellular immunity by FUS sti. spleen, humoral immunity may also be significantly regulated, which represents one dominant factor in the anticancer process during FUS irradiation. Herein, we selectively detected the cytokine levels of GM-CSF, TNF-alpha, IL-12, CCL2, IL-1beta, IL-2, IL-4, IL-6, IL-10, IL-13, IL-17, IFN-gamma, CXCL10, M-CSF, IL-1alpha, CCL4, CXCL12, IL-27, perforin and granzyme in the peripheral blood using the Luminex xMAP technology. Interestingly, the concentration levels of TNF-alpha, IFN-γ, perforin and granzyme were significantly increased in the FUS sti. spleen group as compared with the control group in both H22 and Hepa1-6 HCC in situ models (Figure 3A–C), which indicated the activation of cytotoxic CD8 T cells and NK cells against tumor. Usually, the naive CD8 T cells in the immune process undergo activation and clone expansion, which in turn produce the effector cytokine TNF-alpha, IFN-gamma, perforin and granzyme.[45,46] In addition, the secretion level of IFN-gamma, perforin and granzyme specifically indicated the activation of NK cells to fight cancer.[47]

The concentration levels of the pro-inflammatory chemokines CCL2, CCL4 and CXCL10 were significantly elevated in the FUS sti. spleen group of both orthotopic H22 and Hepa1-6 HCC models compared with those in the control group (Figure 3A–C). These pro-inflammatory chemokines promote immune cells especially effector T cells successfully migrating into metastatic tumor sites to perform an anti-tumor activity.[48–50] CXCL12 is a homeostatic chemokine involved in physiological processes like embryogenesis, neurogenesis, cardiogenesis, hematopoiesis, leukocyte homing, and angiogenesis, by inducing the migration and activation of hematopoietic progenitor and stem cells, endothelial cells, and most leukocytes.[51,52] In this study, the CXCL12 level was significantly increased in the FUS sti. spleen group (Figure 3A–C). As a final level of activity regulation, CXCL12 synergizes with CXCL8 but also with CXCL9, CXCL10, CXCL11, and multiple CC chemokines to attract B- and T-lymphocytes, DCs, monocytes, and $CD34^+$ progenitor cells.[53]

Table 2. Statistical Significance of FCM Results of Immune Cells in the Spleen, Blood, Tumor and Para-Carcinoma Tissue From Orthotopic HCC Mice Subjected to FUS Sti. Spleen or Non-Treated Mice

Analysis	CD4 T cells	Th1 cells	Th2 cells	Th17 cells	B cells	NK cells	CD8 T cells	Mφ	Mφ1	Mφ2	DC1	DC2	Treg cells	M-MDSCs	PMN-MDSCs
Spleen S2 vs. S1	—	**	*	—	—	*	*	*	*	*	*	—	***	*	*
Blood S2 vs. S1	—	—	—	*	*	**	*	—	**	—	**	—	—	—	**
Tumor S2 vs. S1	**	—	—	—	—	**	*	**	*	—	*	—	*	—	*
Liver S2 vs. S1	—	*	—	—	—	*	**	***	***	—	—	—	—	—	*
Spleen L2 vs. L1	—	—	**	*	—	**	*	**	—	—	***	***	*	—	*
Blood L2 vs. L1	*	—	*	*	—	*	**	—	**	*	**	—	—	*	*
Tumor L2 vs. L1	—	—	—	**	—	**	*	*	*	*	*	**	*	—	**
Liver L2 vs. L1	—	—	—	—	—	*	**	*	**	*	—	—	—	—	*

Notes: S1, control group of xenograft H22 HCC in situ; S2, FUS sti. Spleen-treated orthotopic H22 HCC. L1, control group of xenograft Hepa1-6 HCC in situ; L2, FUS sti. Spleen-treated orthotopic Hepa1-6 HCC (n = 4; * $p \le 0.05$; ** $p \le 0.01$; *** $p \le 0.001$). The red asterisk indicates a significant increase in the proportion of immune cells; the blue asterisk indicates a significant decrease in the proportion of immune cells; and the dash represents no significant difference. The representative FCM plots and statistical diagram of immune cells in the S1 and S2 group are shown in Supplementary Figures 3–6, and those in the L1 and L2 group are shown in Supplementary Figures 7–10.

Moreover, CXCL12 binding to its receptor CXCR4 mediates the biological behavior of tumor cells such as movement, chemotaxis, adhesion, secretion (such as MMPs and VEGF), angiogenesis, growth, and proliferation by activating various signaling pathways.[54,55]

Besides, GM-CSF and M-CSF are 2 important cytokines that regulate macrophage population and function. Many experimental loads of evidence suggest that the aberrant expression of GM-CSF and its receptors are present in many cancers such as glioblastoma, small cell carcinoma, skin carcinoma, meningiomas, colon cancer, lung cancer, and particularly HCC, promoting cancer progression by regulating the tumor microenvironment involving Mφ and MDSCs, and promoting epithelial to mesenchymal transition, angiogenesis, and expression of immune checkpoint molecules.[56–59] The concentration level of GM-CSF in this study was significantly decreased as both orthotopic H22 and Hepa1-6 HCC mouse models underwent FUS sti. spleen (Figure 3A–C). In addition, the M-CSF level was increased after orthotopic HCC mice were subjected to FUS sti. spleen (Figure 3A–C), which regulated the survival, proliferation and differentiation of the monocyte-macrophage lineage from progenitors to mature cells and activated several important functions of mature tissular Mφ.[60,61]

The proinflammatory cytokine IL-1beta showed an association with tumor progression,[62] but interestingly, although the inhibition of IL-1beta signaling has potent anti-metastatic effects, the inhibition of the activity of this cytokine has contradictory effects on primary tumors, sometimes reducing but often promoting their growth.[63] Moreover, anti-cancer treatments are able to promote IL-1beta production by cancer or immune cells, with opposite effects on cancer progression,[64] which resembles the tumor-suppressing effect of FUS sti. spleen. However, beyond that, the cytokine levels of IL-1alpha, IL-17 and IL-27 showed no significant differences in consistency as orthotopic H22 and Hepa1-6 HCC mice subjected to FUS sti. spleen (Figure 3A–C). In addition, IL-2 is a pleiotropic cytokine required for both effector lymphocyte proliferation/differentiation and regulatory T cell expansion/survival,[65] which was significantly secreted as spleen responded to FUS stimulation (Figure 3A–C). Additionally, IL-4 mainly secreted by T cells and NK cells induces Mφ2 activation, and regulates the expression of IL-6, IL-10, IL-12 and IL-13.[66] Some studies also reported that polarized Th1 cells produced IL-2, IL-12 and IFN-gamma, and polarized Th2 cells secreted IL-4, IL-6, IL-10 and IL-13 that promoted tumor proliferation[67] (Figure 3A–C). In this study, IL-6 level was increased and IL-13 level was decreased when the orthotopic HCC mice were subjected to FUS sti. spleen (Figure 3A–C). Nevertheless, the

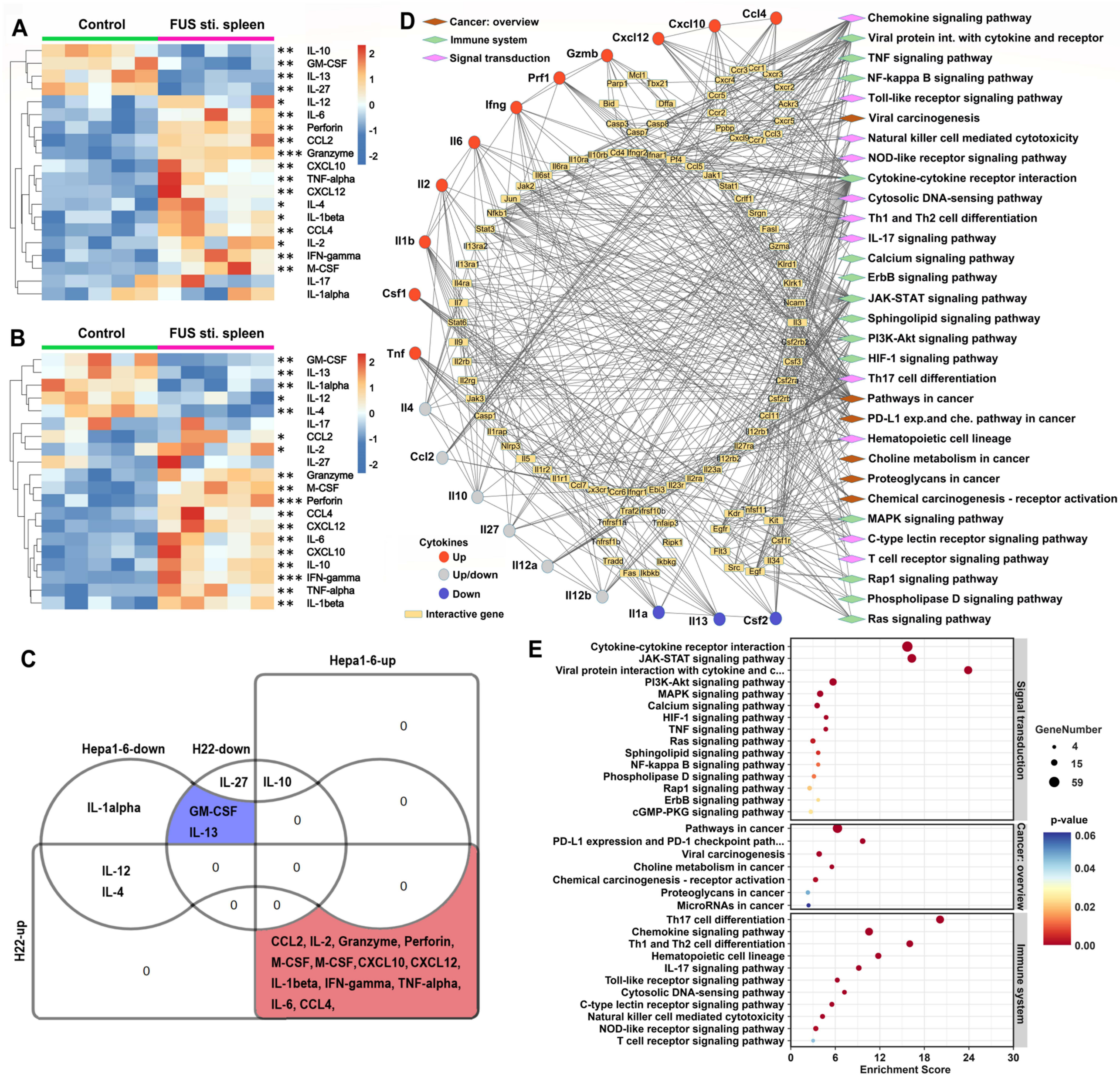

Figure 3 Cytokine detection and bioinformatics analysis. (**A** and **B**), heatmap of cytokine levels in orthotopic H22 and Hepa1-6 HCC mice subjected to FUS sti. spleen. (n = 5; * p ≤ 0.05; **p ≤ 0.01; ***p ≤ 0.001; mean ± SEM). (**C**) Venn diagram of up- and down-regulated cytokines in both orthotopic H22 and Hepa1-6 HCC mice subjected to FUS sti. spleen. (**D**) protein-protein network analysis of cytokines and target genes based on STRING database. (**E**) KEGG pathway enrichment analysis of cytokines and target genes.

cytokine levels of IL-4, IL-10 and IL-12 were altered between orthotopic H22 and Hepa1-6 HCC mice models subjected to FUS sti. spleen (Figure 3A–C).

Protein–protein networks of these cytokines and target genes, and KEGG pathway enrichment analysis showed that FUS stimulating splenic immune cells to regulate cytokines against tumor was associated with several signaling pathways, especially JAK-STAT signaling pathway and PI3K-AKT signaling pathway (Figure 3D and E). It was evident that these cytokines characterized the tumor cytotoxicity of NK cells and CD8 T cells, mainly through cytokine-cytokine receptor interaction pathway to obtain an anticancer effect (Figure 3D and E).

 https://doi.org/10.2147/ITT.S534444

FUS Directly Activated Splenic Immune Cells for Cancer Immunotherapy

FUS Promoted Splenic Positive Immune Cell Proliferation and Activation to Combat Tumor

According to previous studies, splenic ultrasound stimulation activated CAP to inhibit arthritis, colitis, hyperglycemia and other inflammatory diseases, but they paid more attention to the modulation of inflammatory factors such as TNF-α, IL-6 and IL-10, as well as CAP validation, but not to the changes of immune cells.[23,68,69] In this study, FUS sti spleen significantly altered the proportion of immune cells in the spleen, blood, and tumor, especially NK cells and CD8 T cells that increased uniformly in various tumor models (Table 2, Supplementary File 1), thus arousing our special attention. Inexplicably, the previous studies based on inflammatory disease models (eg, pneumonia, myocarditis, and colitis) proved that splenic ultrasound stimulation activates CAP to reduce Mφ and inhibits the secretion of pro-inflammatory cytokines (eg TNF-α), but in this study based on tumor models, FUS sti. spleen significantly increased Mφ and promoted TNF-α secretion. Therefore, our speculation was that FUS directly stimulated splenic immune cells stressing tumor signals, which promoted the proliferation and activation of positive immune cells (ie NK cells and $CD8^+$ T cells) to suppress cancer cell proliferation. To further confirm this hypothesis, splenic nerve blockade was performed with propranolol hydrochloride targeting CAP to explore the impact of CAP deficiency on tumor suppression during FUS sti. spleen. Subsequently, NK cells and CD8 T cells were depleted with Ultra-LEAF™ purified anti-mouse NK-1.1 antibody and Ultra-LEAF™ purified anti-mouse CD8a antibody, respectively, to further explore their role and importance in the tumor-suppressing process of FUS sti. spleen. Forty-eight orthotopic H22 HCC mice were randomly divided into eight groups: the Q1 group was used as the control group; the Q2 group was subjected to FUS sti. spleen; the Q3 group was treated with an intraperitoneal injection of propranolol hydrochloride to block CAP; the Q4 group was subjected to FUS sti. spleen after an intraperitoneal injection of propranolol hydrochloride; the Q5 group was subjected to NK cell clearance; the Q6 group was subjected to FUS sti. spleen after NK cell depletion; the Q7 group was subjected to CD8 T cell clearance; the Q8 group was subjected to FUS sti. spleen after CD8 T cell depletion. The operation of FUS sti. spleen and experimental timeline were identical to those described in Figure 2A.

The therapeutic results once again demonstrated the significant tumor suppression of FUS sti. spleen (Q2 vs Q1, $p < 0.001$; Figure 4A–C). It is noteworthy that specifically CAP blockage did not significantly attenuate the therapeutic efficacy of FUS sti. spleen on the tumor (Q4 vs Q3, $p < 0.001$; Figure 4A–C), although the anti-tumor rate was slightly reduced in the Q4 group as compared to the Q2 group. It confirmed our previous speculation that CAP did not play a dominant role in the process of FUS sti. spleen for tumor suppression. We supposed that cancer is different from inflammatory diseases such as arthritis, colitis, and pneumonia, and FUS sti spleen to inhibit inflammatory diseases mainly relied on CAP affecting humoral immunity, while it suppressed tumor proliferation mainly depending on the direct modulation of cellular immunity.

Furthermore, the tumor proliferation was significantly promoted after NK cell depletion (Q5 vs Q1, $p < 0.001$; Figure 4A–C). Interestingly, FUS sti. spleen did not show any tumor suppressive effect after depleting NK cells (Q6 vs Q5; Figure 4A–C). Moreover, CD8 T cell clearance promoted tumor proliferation (Q7 vs Q1, $p<0.05$; Figure 4A–C), but as opposite as NK cell clearance, did not reduce the therapeutic efficacy of FUS sti. spleen on tumor (Q8 vs Q2; Figure 4A–C). These results proved that NK cells were much more indispensable and important in cancer suppression in response to FUS stimulation than CD8 T cells. The statistical results of liver weight, mice weight, spleen weight and spleen index also showed that NK cell depletion had a significant effect on tumor proliferation and splenomegaly, and elucidated the attenuation of FUS sti. spleen on tumor suppression and splenomegaly (Figure 4D–G).

The concentration of NE and ACh in the plasma was significantly increased after FUS sti. spleen (Q2 vs Q1, Q6 vs Q5, and Q8 vs Q7, $p < 0.05$; Figure 4H and I), which indicated that FUS sti. spleen indeed activated splenic CAP. In addition, propranolol hydrochloride significantly blocked the binding of NE to adrenergic receptors, that is, effectively blocking CAP, thus increasing the NE content (Q3 vs Q1, $p<0.01$; Figure 4H) but no significant changes in ACh (Q3 vs Q1; Figure 4I). Therefore, NE content increased after FUS sti. spleen (Q4 vs Q3; Figure 4H), while ACh did not significantly change (Q4 vs Q3; Figure 4I). Nevertheless, it is important to note that the results of granzyme and perforin detection by ELISA further confirmed the significance of splenic NK cells activation and their secreting cytotoxic molecules in response to FUS stimulation for an anti-cancer effect, but not affected by CAP (Figure 4J and K).

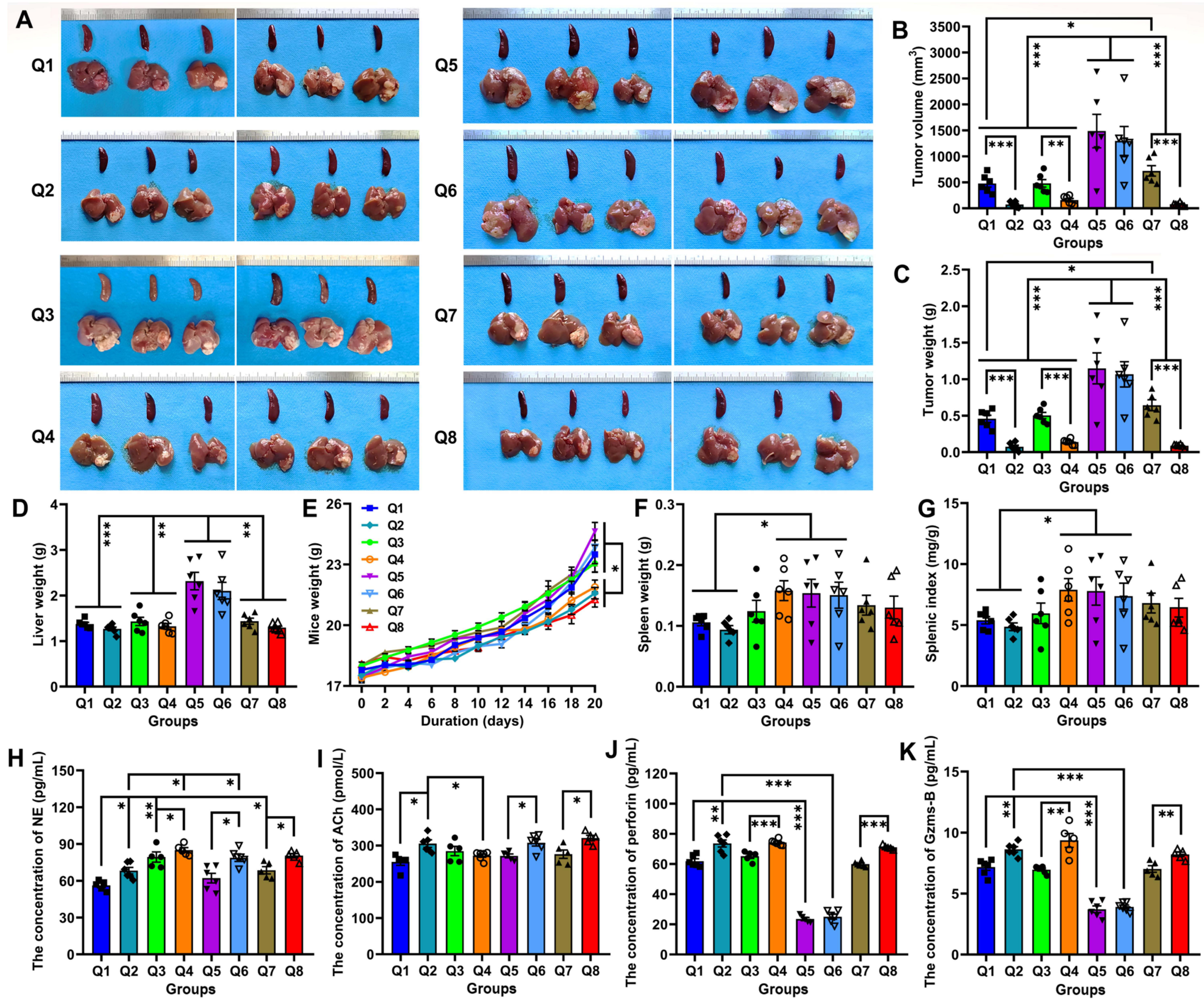

Figure 4 Therapeutic effect of FUS sti. spleen on xenograft H22 carcinoma in situ after CAP blockage, NK cells depletion and CD8 T cell clearance. (**A**) images of spleen and orthotopic H22 tumor. (**B** and **C**) tumor volume and tumor weight, respectively. (**D–F**) liver weight, mice weight and spleen weight, respectively. **G**, splenic index calculated by the ratio of spleen weight to mouse weight. (**H–K**) concentration of NE, ACh, granzyme and perforin, respectively, detected by ELISA. (n = 6; * p ≤ 0.05; **p ≤ 0.01; ***p ≤ 0.001; mean ± SEM). Q1, control group of xenograft H22 HCC in situ; Q2, FUS sti. spleen on day 2 after H22 cancer cell implantation; Q3, injection of propranolol hydrochloride to block CAP; Q4, FUS sti. spleen after injection of propranolol hydrochloride; Q5, NK cell clearance; Q6, FUS sti. spleen after NK cell depletion; Q7, CD8 T cell clearance; Q8, FUS sti. spleen after CD8 T cell depletion.

FCM results proved that Ultra-LEAF™ purified anti-mouse NK-1.1 antibody and Ultra-LEAF™ purified anti-mouse CD8a antibody effectively eliminated NK cells and CD8 T cells in the body, respectively (Q5/6 and Q7/8 vs Q1/2; Tables 3–6, Supplementary Figures 11–14). In the case of CAP blockage and NK or CD8 T cell clearance, the proportion of Mφ, DCs and MDSCs in the body was also affected, especially the number of Mφ and DCs that was generally reduced after depleting NK cells and CD8 T cells (Q3/4, Q5/6 and Q7/8 vs Q1/2; Tables 3–6, Supplementary Figures 11–14). However, FUS sti. spleen consistently increased the number of NK cells and CD8 T cells in the body regardless of CAP blockade and NK or CD8 T cell clearance, followed by Mφ1 and DC1 (Q4 vs Q3, Q6 vs Q5, and Q8 vs Q7; Tables 3–6, Supplementary Figures 11–14), while the variation tendency of other immune cells (including PMN-MDSCs) was not consistent in the spleen, blood, tumor and para-carcinoma tissue (Tables 3–6, Supplementary Figures 11–14). Clearly, changes in the proportion of immune cells (especially NK cells) with or without modulation by splenic ultrasound stimulation were closely related to the anti-tumor effect.

The results of the above CAP blockage experiments demonstrated that CAP did not play a dominant role in tumor suppression by FUS sti. spleen; however, it could not exclude the impact of splenic nerve or other nerve signals.

Table 3. FCM Results of Immune Cells in the Spleen

Analysis	NK cells	$CD8^+$ T cells	Mφ	Mφ1	Mφ2	DC1	DC2	Treg cells	M-MDSC	PMN-MDSC
Q2 vs. Q1	**	*	**	*	**	**	—	—	**	**
Q4 vs. Q3	**	*	*	*	***	*	**	—	**	—
Q6 vs. Q5	—	—	—	—	—	**	—	—	**	—
Q8 vs. Q7	**	*	—	*	**	**	*	—	*	—
Q3 vs. Q1	—	—	*	—	—	*	—	—	—	—
Q4 vs. Q2	—	—	*	—	—	*	*	—	—	—
Q5 vs. Q1	***	*	***	—	**	*	—	*	—	—
Q6 vs. Q2	***	*	***	—	—	*	—	—	—	—
Q7 vs. Q1	—	**	—	—	—	**	*	—	*	—
Q8 vs. Q2	—	**	*	—	—	**	—	—	—	—

Notes: Q1, control group of xenograft H22 HCC in situ; Q2, FUS sti. spleen; Q3, injection of propranolol hydrochloride to block CAP; Q4, FUS sti. spleen after injection of propranolol hydrochloride; Q5, NK cell clearance; Q6, FUS sti. spleen after NK cell depletion; Q7, CD8 T cell clearance; Q8, FUS sti. spleen after CD8 T cell depletion (n = 4; * $p \le 0.05$; **$p \le 0.01$; ***$p \le 0.001$). The red asterisk indicates a significant increase in the number of immune cells; the blue asterisk indicates a significant decrease in the number of immune cells; and the dash represents no significant difference. The representative FCM plots and statistical diagram of immune cells in the Q1-8 groups are shown in Supplementary Figure 11.

Table 4. FCM Results of Immune Cells in the Blood

Analysis	NK cells	$CD8^+$ T cells	Mφ	Mφ1	Mφ2	DC1	DC2	Treg cells	M-MDSC	PMN-MDSC
Q2 vs. Q1	**	**	—	*	—	*	**	**	—	*
Q4 vs. Q3	**	—	**	—	—	*	***	—	*	**
Q6 vs. Q5	—	**	—	—	—	**	*	—	—	—
Q8 vs. Q7	**	***	*	—	*	***	—	**	—	**
Q3 vs. Q1	—	—	—	—	—	—	—	—	**	—
Q4 vs. Q2	—	*	**	—	—	*	—	***	*	**
Q5 vs. Q1	***	—	—	**	—	**	***	—	*	***
Q6 vs. Q2	***	—	—	**	—	—	—	**	—	**
Q7 vs. Q1	—	***	—	—	—	***	—	—	**	—
Q8 vs. Q2	—	**	*	—	**	—	*	—	—	***

Notes: Q1, control group of xenograft H22 HCC in situ; Q2, FUS sti. spleen; Q3, injection of propranolol hydrochloride to block CAP; Q4, FUS sti. spleen after injection of propranolol hydrochloride; Q5, NK cell clearance; Q6, FUS sti. spleen after NK cell depletion; Q7, CD8 T cell clearance; Q8, FUS sti. spleen after CD8 T cell depletion (n = 4; * $p \le 0.05$; **$p \le 0.01$; ***$p \le 0.001$). The red asterisk indicates a significant increase in the number of immune cells; the blue asterisk indicates a significant decrease in the number of immune cells; and the dash represents no significant difference. The representative FCM plots and statistical diagram of immune cells in the Q1-8 groups are shown in Supplementary Figure 12.

Thereafter, we applied absolute ethanol to denervate the splenic nerve to explore the role of the splenic nerve on spleen immunomodulation and anti-cancer effect by FUS sti. spleen. Moreover, the spleen was removed to exclude the possibility of immune regulation and tumor suppression by FUS irradiation on non-splenic organs or tissues. Thus, forty-two orthotopic H22 HCC mice were randomly divided into six groups: H1 group was used as the control group; H2

Table 5. FCM Results of Immune Cells in the Tumor

Analysis	NK cells	$CD8^+$ T cells	Mφ	Mφ1	Mφ2	DC1	DC2	Treg cells	M-MDSC	PMN-MDSC
Q2 vs. Q1	*	**	*	—	—	—	—	—	**	*
Q4 vs. Q3	**	**	*	—	**	—	—	*	—	—
Q6 vs. Q5	—	*	—	—	—	*	**	—	—	—
Q8 vs. Q7	*	***	*	**	*	*	—	—	—	**
Q3 vs. Q1	—	—	—	—	—	—	—	—	**	—
Q4 vs. Q2	—	—	—	—	**	**	—	—	**	—
Q5 vs. Q1	***	—	—	**	***	**	***	***	***	—
Q6 vs. Q2	***	—	*	**	**	—	—	***	***	—
Q7 vs. Q1	—	*	—	*	—	—	—	—	—	*
Q8 vs. Q2	—	—	—	—	—	—	—	—	**	—

Notes: Q1, control group of xenograft H22 HCC in situ; Q2, FUS sti. spleen; Q3, injection of propranolol hydrochloride to block CAP; Q4, FUS sti. spleen after injection of propranolol hydrochloride; Q5, NK cell clearance; Q6, FUS sti. spleen after NK cell depletion; Q7, CD8 T cell clearance; Q8, FUS sti. spleen after CD8 T cell depletion (n = 4; * $p \le 0.05$; ** $p \le 0.01$; *** $p \le 0.001$). The red asterisk indicates a significant increase in the number of immune cells; the blue asterisk indicates a significant decrease in the number of immune cells; and the dash represents no significant difference. The representative FCM plots and statistical diagram of immune cells in Q1-8 groups are shown in Supplementary Figure 13.

Table 6. FCM Results of Immune Cells in Para-Carcinoma Tissue

Analysis	NK cells	$CD8^+$ T cells	Mφ	Mφ1	Mφ2	DC1	DC2	Treg cells	M-MDSC	PMN-MDSC
Q2 vs. Q1	*	**	*	**	—	*	—	*	—	*
Q4 vs. Q3	*	*	*	—	—	—	—	*	*	—
Q6 vs. Q5	—	—	*	—	—	*	—	—	—	—
Q8 vs. Q7	*	***	—	*	***	—	—	***	—	**
Q3 vs. Q1	—	—	—	—	***	—	—	—	—	—
Q4 vs. Q2	—	—	—	**	***	—	—	—	**	—
Q5 vs. Q1	***	—	—	—	***	—	**	—	—	—
Q6 vs. Q2	***	—	—	**	***	—	**	*	**	—
Q7 vs. Q1	—	***	*	*	—	***	—	—	—	—
Q8 vs. Q2	—	*	—	*	*	***	—	*	—	**

Notes: Q1, control group of xenograft H22 HCC in situ; Q2, FUS sti. spleen; Q3, injection of propranolol hydrochloride to block CAP; Q4, FUS sti. spleen after injection of propranolol hydrochloride; Q5, NK cell clearance; Q6, FUS sti. spleen after NK cell depletion; Q7, CD8 T cell clearance; Q8, FUS sti. spleen after CD8 T cell depletion (n = 4; * $p \le 0.05$; ** $p \le 0.01$; *** $p \le 0.001$). The red asterisk indicates a significant increase in the number of immune cells; the blue asterisk indicates a significant decrease in the number of immune cells; and the dash represents no significant difference. The representative FCM plots and statistical diagram of immune cells in Q1-8 groups are shown in Supplementary Figure 13.

group was subjected to FUS sti. spleen; H3 group was subjected to splenic nerve denervation by absolute ethanol; H4 group was subjected to FUS sti. spleen after splenic nerve denervation; H5 group was subjected to the removal of the spleen; and H6 group was exposed to FUS on spleen position after splenectomy.

The results showed that splenic nerve denervation promoted tumor proliferation to some extent, although not significant (H3 vs H1, p = 0.3430 in tumor volume and p = 0.1590 in tumor weight), suggesting that the splenic nerve had a certain role in the anti-tumor effect. However, more importantly, splenic nerve denervation did not attenuate the tumor suppression efficacy of FUS sti. spleen, which was up to ~75% (H4 vs H3, p<0.001; Figure 5A–C) that was superior to or consistent with the tumor inhibition rate of FUS sti. spleen without splenic nerve denervation (~70%, H2 vs H1, p<0.001; Figure 5A–C). It further ruled out the indispensable role of splenic nerve on tumor suppression by FUS sti. spleen, which was also direct evidence that FUS directly stimulated splenic immune cells to regulate immunity against cancer.

Liver weight and mice weight also indirectly reflected the anti-cancer effect of FUS sti. spleen after splenic nerve denervation (Figure 5D and E). However, it must be noted that spleen weight and spleen index clearly indicated that splenic nerve denervation dramatically promoted tumor-induced splenomegaly (H3 vs H1, p < 0.01; Figure 5F and G), while FUS sti. spleen significantly reduced splenomegaly (H4 vs H3, p < 0.01; Figure 5F and G). The comprehensive analysis of the changes in splenic characteristics and tumor proliferation showed that the splenic nerve played an important role in the anti-cancer effect of the spleen under the natural state but not the splenic ultrasound stimulation.

ELISA results of NE and ACh showed that splenic neurons were not activated by FUS under splenic nerve denervation; thus, there was no significant change in the concentration of CAP-related NE and Ach (H4 vs H3; Figure 5H and I). The c-Fos immunohistochemical staining also proved that few splenic neurons responded to FUS stimulation after splenic nerve denervation (Figure 5J). However, splenic nerve denervation did not affect the response of splenic immune cells to FUS stimulation, especially the NK cells that secreted significantly higher levels of perforin and granzyme (H4 vs H3, p<0.01; Figure 5K and L). Particularly, after splenectomy, FUS irradiation in splenic position did not show any anti-tumor effect (H6 vs H5; Figure 5A–E, K-L), which demonstrated that the spleen irradiated with FUS was the only cause of the anti-cancer effect, and directly showed that the integrity of spleen was critical during FUS sti. spleen for tumor suppression. In summary, comprehensive analysis of splenectomy and splenic nerve denervation experiments clearly confirmed that FUS activated splenic anticancer immune function through the direct FUS stimulation of immune cells, thus further suppressing tumor proliferation.

FCM results proved that splenic nerve denervation did not affect cell proportion (H3 vs H1; Supplementary Figures 15–18), particularly not weaken the modulation properties of FUS sti. spleen on the increase of the positive immune cells (especially NK cells, CD8 T cells, Mφ1 and DC1) in the body, and decrease of the negative immune cells PMN-MDSCs (H4 vs H2/3; Supplementary Figures 15–18). It fully demonstrated that FUS directly stimulated the splenic immune cells to promote their proliferation and activated the anti-cancer capability. After the removal of the spleen, the proportion of most immune cells in the peripheral blood was significantly decreased (H5/6 vs H1/2; Supplementary Figure 16), which indicated the importance of spleen for the body's immune system. However, after splenectomy, the spleen location irradiated by FUS did not show any impact on the number of immune cells (H6 vs H5; Supplementary Figures 16–18), which demonstrated that the spleen integrity or the presence of immune cells was essential for responding to FUS stimulation in tumor immunotherapy.

Association of Splenic Positive and Negative Immune Cells Responding to FUS Irradiation

Our previous study demonstrated that the proportion of PMN-MDSCs in the spleen and blood from tumor-bearing mice was significantly increased, which suppressed NK cells and CD8 T cells.[70] After FUS sti. spleen, the proportion of positive immune cells such as NK cells and CD8 T cells in the body was significantly increased, while the proportion of negative immune cells such as PMN-MDSCs was significantly decreased (Table 2, Supplementary File 1). Why did FUS, as a non-specific physical method, cause the number of positive and negative immune cells to change in two directions? The depletion of NK cells and CD8 T cells did not show consistent changes of PMN-MDSCs in the spleen and blood (Q5/6 and Q7/8 vs Q1/2; Tables 3 and 4); thus we proposed to reversely demonstrate the association of NK cells and CD8 T cells to PMN-MDSCs by depleting PMN-MDSCs. Forty orthotopic H22 HCC mice were randomly divided into

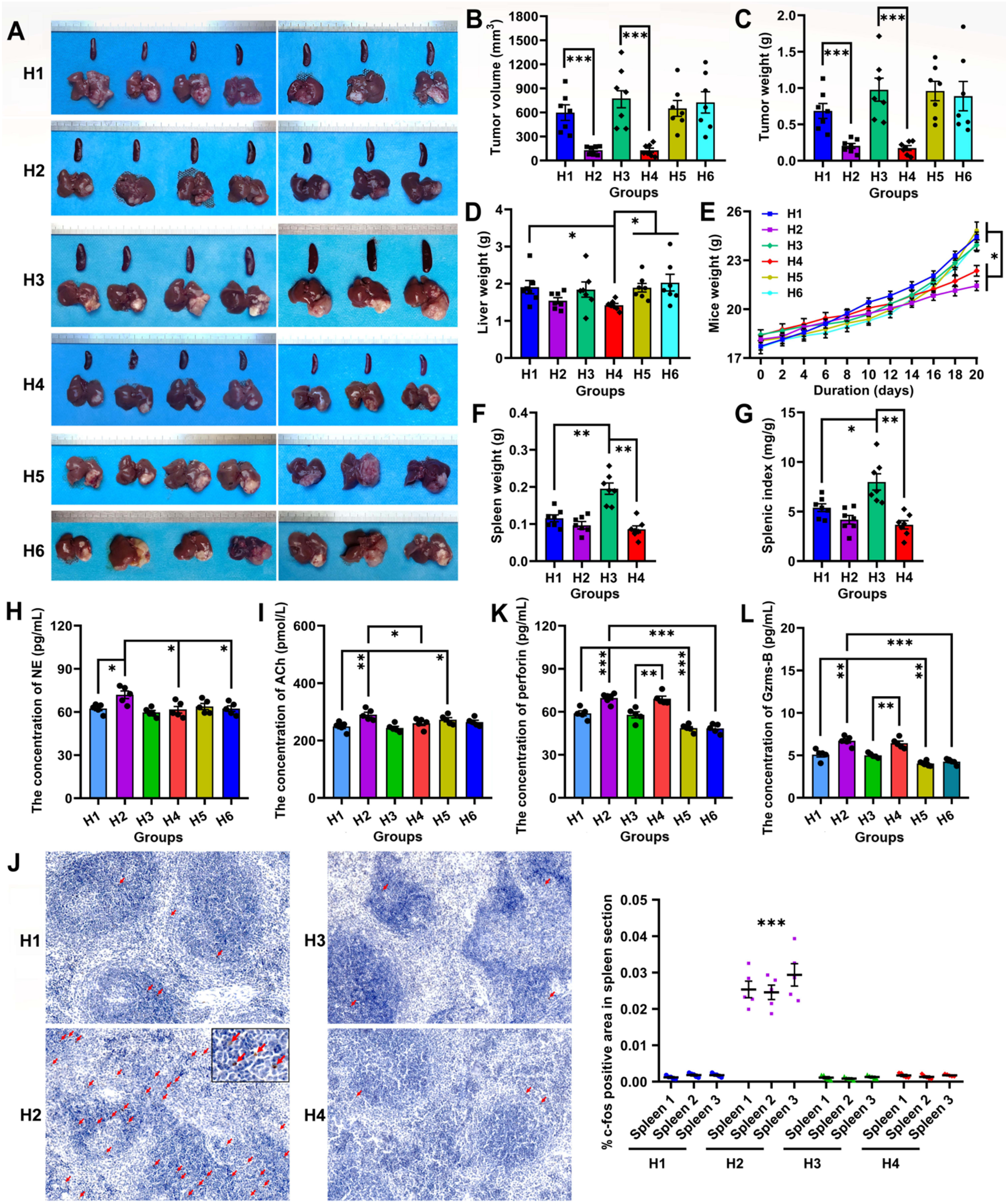

Figure 5 Therapeutic effect of FUS sti. spleen on tumor suppression after splenic nerve denervation and splenectomy. (**A**) images of spleen and orthotopic H22 tumor. (**B** and **C**) tumor volume and tumor weight, respectively. (**D**–**F**) liver weight, mice weight and spleen weight respectively. (**G**) splenic index calculated by the ratio of spleen weight to mouse weight. (n = 7; * p ≤ 0.05; **p ≤ 0.01; ***p ≤ 0.001; mean ± SEM). (**H** and **I**) concentration of NE and ACh, respectively, detected by ELISA. (**J**) c-Fos immunohistochemical staining and statistical result of positive area in section; the red arrows indicate the c-Fos-positive cells. (**K** and **L**) concentration of granzyme and perforin, respectively, detected by ELISA. (n = 5; * p ≤ 0.05; **p ≤ 0.01; ***p ≤ 0.001; mean ± SEM). H1, control group of xenograft H22 HCC in situ; H2, FUS sti. spleen on day 2 after H22 cancer cell implantation; H3, splenic nerve denervation by absolute ethanol; H4, FUS sti. spleen after splenic nerve denervation; H5, removal of the spleen; H6, FUS stimulated the splenic position after splenectomy.

four groups: R1 group was used as the control group; R2 group was subjected to FUS sti. spleen; R3 group was subjected to PMN-MDSCs depletion; and R4 group was subjected to FUS sti. spleen after PMN-MDSCs clearance.

PMN-MDSCs depletion inhibited tumor proliferation to a certain extent (R3 vs R1; Supplementary Figure 19A–D) and the subsequent FUS sti. spleen further enhanced tumor suppression (R4 vs R3; Supplementary Figure 19A–D). However, the tumor suppressive effect of FUS sti. spleen after PMN-MDSCs clearance was slightly weaker than that without PMN-MDSCs depletion (R4 vs R2; Supplementary Figure 19A–C). Mice weight did not clearly show a significant difference among the four groups (Supplementary Figure 19E), but spleen weight and spleen index showed a decreased trend in the R4 group as compared to the R3 group (Supplementary Figure 19Fand G).

FCM results showed that Ultra-LEAF™ purified anti-mouse Ly-6G antibody effectively eliminated PMN-MDSCs from the spleen, blood, tumor, and para-carcinoma tissue (R3 vs R1; Supplementary Figures 19H–K and 20–23). Interestingly, it significantly increased the proportion of Mφ, especially Mφ2, in the spleen and blood (R3 vs R1; Supplementary Figures 19H and I, 20 and 21). Moreover, PMN-MDSC depletion significantly increased NK cells and CD8 T cells only in the blood (R3 vs R1; Supplementary Figures 19I and 21). These results explained the reason that PMN-MDSCs clearance suppressed tumor proliferation to a certain extent (Supplementary Figure 19A–D). Even more important, PMN-MDSC depletion in spleen did not promote the proliferation of splenic NK cells and CD8 T cells (R3 vs R1; Supplementary Figures 19H and 20). Combined with the observation that the depletion of NK cells and CD8 T cells in the spleen did not increase the proportion of splenic PMN-MDSCs (Q5 and Q7 vs Q1; Table 3), it proved that there was no direct interaction between PMN-MDSCs and NK cells or CD8 T cells. Accordingly, it is reasonable to deduce that FUS sti. spleen increased the number of NK cells and CD8 T cells while the decrease of PMN-MDSCs was not directly correlated. PMN-MDSC decrease may be attributed to the increase of other immune cells in the spleen such as Mφ, especially Mφ2 mentioned above, or even to the rise of total tumor suppressor related immune cells in the spleen and blood. Of course, this mechanism has yet to be explored in the light of more direct and conclusive evidence.

FUS Regulating Calcium-Related Signaling Pathways to Modulate Splenic Immunity

The above results revealed that splenic NK cells and CD8 T cells were critical for suppressing tumor growth in response to FUS stimulation. Thereafter, RNA sequencing was performed to verify their changes at the molecular level and investigate the biological mechanism underlying this phenomenon.

According to the differential gene expression clustering heatmap and volcano plot, 655 upregulated genes and 344 downregulated genes were found in NK cells (Supplementary Figure 24A–C), as well as 1869 upregulated genes and 877 downregulated genes in CD8 T cells (Supplementary Figure 24A–C) in the FUS sti. spleen group compared with the control group (Supplementary Figure 24D–F). Both GO and KEGG enrichment analysis showed that the DEGs were significantly enriched in pathways of cell adhesion, cell migration, immune process (ie ECM-receptor interaction, antigen processing and presentation, and intestinal immune network for IgA production) and signal transduction (ie PI3K-AKT signaling pathway, Rap1 signaling pathway, Hippo signaling pathway and calcium signaling pathway) in the FUS sti. spleen group compared with the control group (Supplementary Figure 24G–N).

Further analysis revealed that genes related to NK cell immune function, especially activation, proliferation, and motility, were significantly up-regulated after FUS sti. spleen (Supplementary Figure 25A–C). Genes involved in calcium-related signaling pathways were also significantly highly expressed (Supplementary Figure 25D). According to GO functional annotation analysis, these upregulated genes were not only involved in the positive regulation of cell proliferation, migration and kinase activity, but also mainly involved in integrin-mediated signaling pathway and epidermal growth factor receptor signaling pathway (Supplementary Figure 26A). Moreover, MHC class II protein complex was suppressed (Supplementary Figure 26B), which promoted NK cell activation in mice as reported by Li et al.[71] Particularly, KEGG enrichment analysis of these upregulated genes showed the upregulation of PI3K-Akt signaling pathway, Hippo signaling pathway, ErbB signaling pathway, and Ras signaling pathway (Supplementary Figure 26C), which were closely associated with cell proliferation, differentiation and activation, especially under ultrasound stimulation.[72–74] Downregulated genes were significantly enriched in the intestinal immune network for IgA production (Supplementary Figure 26D), which might be beneficial to tumor suppression as previous studies reported that IgA inhibits NK activity of NK cell-enriched lymphoid cells and gamma-interferon-treated effector cells.[75,76]

More importantly, protein-protein networks revealed that among these significantly different signaling pathways, it is likely that the calcium signaling pathway played a central role and affected the expression of other signals to promote NK cell proliferation, migration and activation (Supplementary Figure 26E). Furthermore, GSEA analysis confirmed that FUS stimulation significantly regulated various signaling pathways of NK cells, such as up-regulating ECM-receptor interaction, PI3K-AKT signaling pathway, Hippo signaling pathway and calcium signaling pathways (Supplementary Figure 26F).

Additionally, the genes related to CD8 T cell activation, proliferation, and motility were significantly up-regulated in the FUS sti. spleen group compared to the control group (Supplementary Figure 27E–G). Genes involved in calcium-related signaling pathways were also highly expressed (Supplementary Figure 27H). GO and KEGG enrichment and network analysis of the differential genes showed significant enrichment of pathways in signal transduction (ie Rap1 signaling pathway, MAPK/ERK signaling pathway, and calcium-related signaling pathways) and immune process (ie IL-6 production, IgA production, Fc epsilon RI signaling pathway and Fc gamma R-mediated phagocytosis) (Supplementary Figure 28A–D). Particularly, the calcium signaling pathway was involved in regulating most of the others and it was probably the initial response to FUS stimulation (Supplementary Figure 28E). GSEA analysis proved that these signaling pathways involving CD8 T cells proliferation, activation and migration, such as ECM-receptor interaction, PI3K-AKT signaling pathway, Rap1 signaling pathway and calcium signaling pathways were significantly upregulated (Supplementary Figure 28F). Although the GO and KEGG enrichment analysis of the downregulated genes showed the downregulation of MAPK signaling pathway, TNF signaling pathway and others (Supplementary Figure 28D), GSEA analysis revealed that these signaling pathways were highly expressed when the tumor-bearing mice were subjected to FUS sti. spleen (Supplementary Figure 28G).

These functional annotations suggested that FUS first activated calcium-related signaling pathways and then regulated other signaling pathways to promote the proliferation, activation, and migration of NK cells and CD8 T cells. Many previous studies confirmed that ultrasound affects the proliferation, activation, and differentiation of various cells by altering intracellular calcium-related signaling pathways to achieve specific biological effects.[77–79] The further exploration of splenic calcium changes in response to FUS stimulation by the Von Kossa staining and FCM detecting Fluo-4 AM labeled cells revealed that the splenic cell population of Von Kossa stained and Fluo-4 AM labeled were observably increased in the FUS sti. spleen group as compared with the control group (Figure 6A and B). Calcium deposits in spleen can promote cytokine production, such as Mφ secreting IL-1β and TNF-α.[80,81] Particularly, the results of in vitro experiments (Figure 6C) fully demonstrated that FUS stimulation promoted NK cell proliferation and activation to suppress cancer cell deterioration (note: H22 cancer cells were unable to adhere to the bottom and difficult to separate from NK cells that migrated from the upper layer of the transwell to the bottom layer, which led to a significant error in the subsequent detection results. Thus, Hepa1-6 cancer cells were chosen for the in vitro study). Moreover, calcium strengthened the impact of FUS stimulation on splenic NK cells to suppress the proliferation of cancer cells in vitro (Figure 6C). Besides, ultrasound shattered cancer cell suspension further enhanced the anticancer effect of calcium-involved FUS simulation on splenic NK cells. Additionally, we also verified that calcium reinforced the effect of FUS stimulation on splenic CD8 T cells to suppress cancer cell deterioration in vitro (not supplying the data). Overall, the above experimental results succinctly proved that FUS altered calcium-related signaling pathways in NK cells and CD8 T cells to reinforce the antitumor effect. However, in the future, it is worthwhile comprehensively and systematically analyzing the specific mechanism of splenic immune cells in response to FUS stimulation by spatial region-resolved proteome and spatial single-cell sequencing.

Therapeutic Application of FUS Sti. Spleen on Intermediate and Advanced Tumors

The above studies in which FUS sti. spleen was performed on the second day after cancer cells implanted into the mice were equivalent to the start of the treatment in the early stage of cancer (before tumor formation). However, the anticancer effect of FUS sti. spleen after tumor formation is one of the worthiest explorations in clinical transformation and application. Therefore, a comparative study was performed to investigate the therapeutic application of FUS sti. spleen on 5th and 9th day after H22 cancer cell transplantation into the liver deemed to be tumorigenesis (Figure 7A). Four experimental groups were set as follows: K1 group was used as the control group of xenograft H22 HCC in situ;

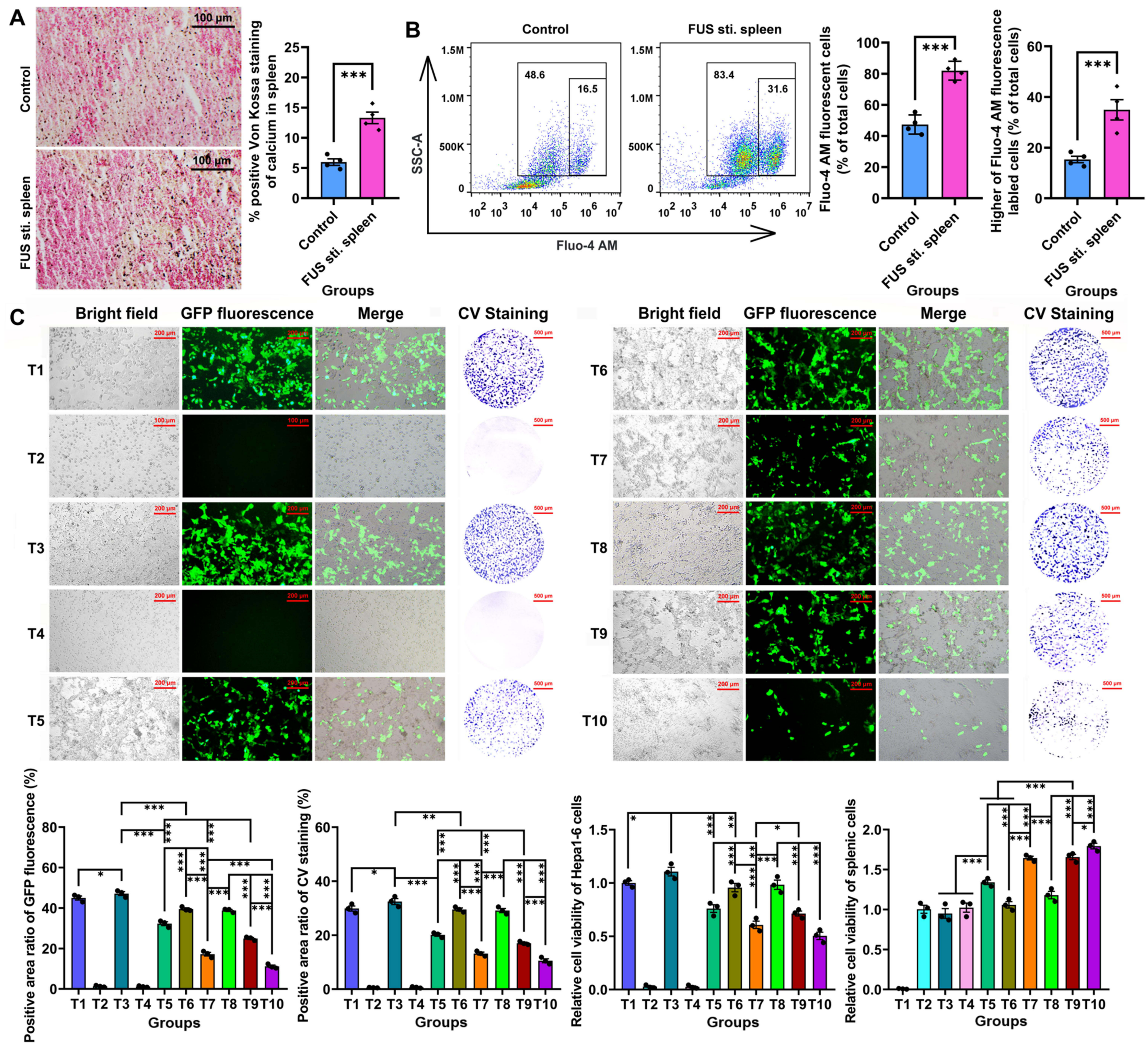

Figure 6 Calcium strengthened FUS-stimulated splenic NK cells against Hepa1-6 cancer cells. (**A**) Von Kossa staining of calcium deposition in the spleen with or without FUS stimulation. (**B**) FCM detected Fluo-4 AM labeled cells in the spleen with or without FUS stimulation. (n = 4; * p ≤ 0.05; **p ≤ 0.01; ***p ≤ 0.001; mean ± SEM). (**C**) results of calcium strengthened impact of FUS stimulation on splenic NK cells to suppress cancer cells in vitro, including GFP fluorescence imaging, CV staining and CCK-8 assay to analyze the proliferation and activity of Hepa1-6 cancer cells, and CCK-8 assay to characterize the proliferation and cytoactivity of NK cells. (n = 3; * p ≤ 0.05; **p ≤ 0.01; ***p ≤ 0.001; mean ± SEM). T1, Hepa1-6 cancer cells; T2, NK cells; T3, NK cells cocultured with Hepa1-6 cancer cells in the transwell; T4, FUS stimulated NK cells; T5, NK cells subjected to FUS irradiation, and then cocultured with Hepa1-6 cancer cells in the transwell; T6, NK cells mixed with Hepa1-6 lysate and cocultured with Hepa1-6 cancer cells in the transwell; T7, NK cells mixed with Hepa1-6 lysate, subjected to FUS irradiation, and then cocultured with Hepa1-6 cancer cells in the transwell; T8, NK cells mixed with Hepa1-6 lysate in 300 nM calcium culture medium and cocultured with Hepa1-6 cancer cells in the transwell; T9, NK cells in 300 nM calcium culture medium subjected to FUS irradiation, and then cocultured with Hepa1-6 cancer cells in the transwell; T10, NK cells mixed with Hepa1-6 lysate in 300 nM calcium culture medium, subjected to FUS irradiation, and then cocultured with Hepa1-6 cancer cells in the transwell.

K2-K4 groups were subjected to FUS sti. spleen on days 0, 4 and 8 after H22 cancer cell implantation, and once every two days (Figure 7A). At the experimental endpoint (day 21), animals underwent terminal anesthesia followed by comprehensive tissue harvesting for other experimental analyses (eg, FCM).

The results showed that FUS sti. spleen on day 0, 4 and 8 significantly suppressed the proliferation of xenograft H22 HCC carcinoma in situ, with an anti-tumor rate of up to ~70%, ~67% and ~48% respectively (K2/3/4 vs K1; Figure 7B–D). The results tautologically demonstrated that FUS sti. spleen exerted an evident tumor suppression, regardless of being performed before or after tumorigenesis, but the later ultrasound irradiation on the spleen was performed after the onset

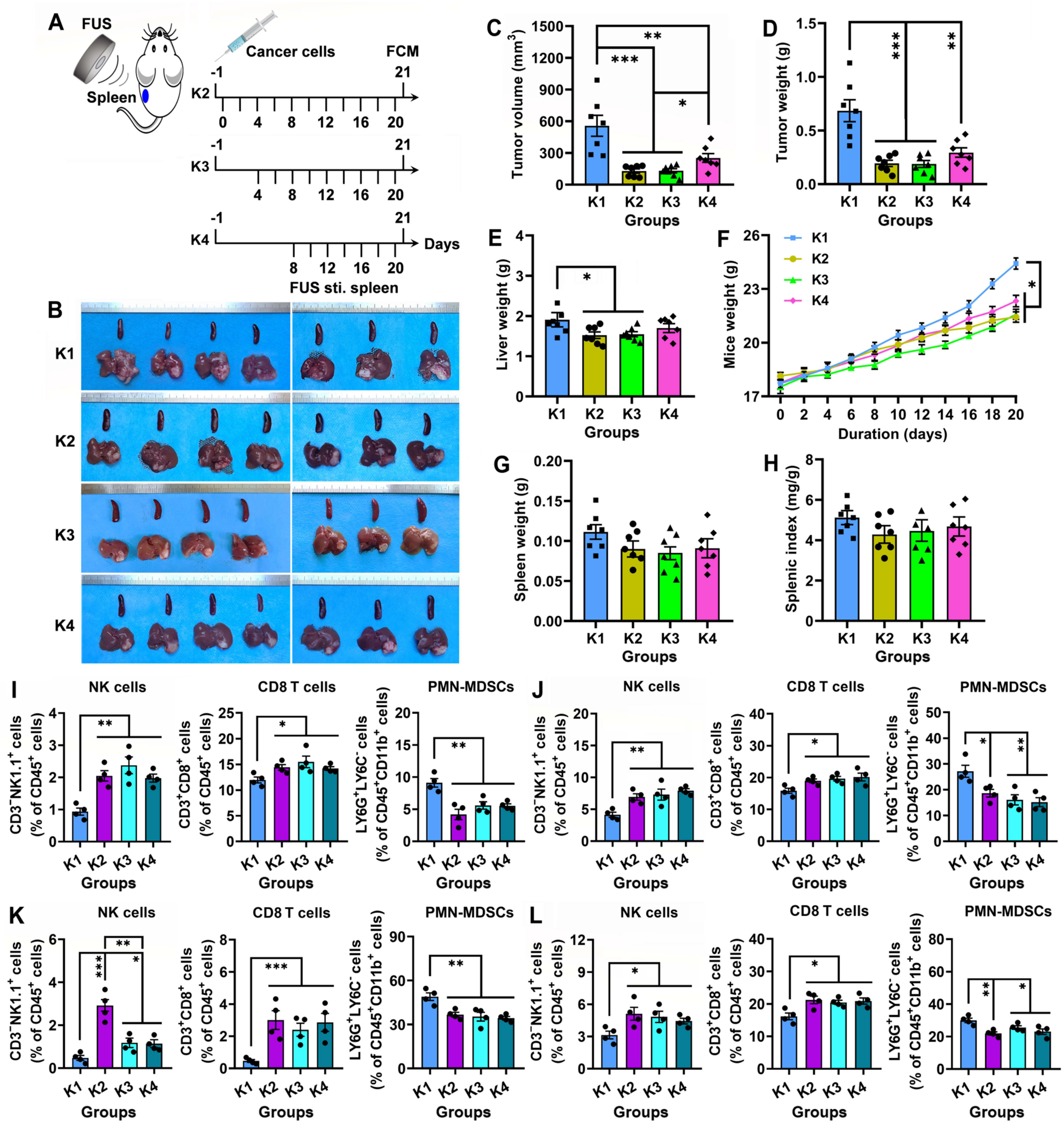

Figure 7 FUS sti. spleen suppressed the proliferation of the xenograft H22 HCC in situ. (**A**) experimental flow diagram of FUS sti. spleen on day 0, 4 and 8 after H22 cancer cell implantation. (**B**) images of spleen and xenograft H22 HCC in situ. (**C**) tumor volume. (**D**) tumor weight. (**E**) liver weight. (**F**) curve of mice weight. (**G**) spleen weight. (**H**) spleen index calculated by the ratio of spleen weight to mouse weight. (n = 7; * p ≤ 0.05; **p ≤ 0.01; ***p ≤ 0.001; mean ± SEM). (**I–L**), FCM results of NK cells, CD8 T cells and PMN-MDSCs in the spleen, blood, tumor, and para-carcinoma tissues, respectively. (n = 4; * p ≤ 0.05; **p ≤ 0.01; ***p ≤ 0.001; mean ± SEM). K1, control group of xenograft H22 HCC in situ; K2-K4, FUS sti. spleen on day 0, 4 and 8, respectively, after H22 cancer cell implantation. Representative FCM plots and statistical diagram of immune cells in K1-K4 groups are shown in Supplementary Figures 29–32. The results shown in Figures 7 and 5 were from the same batch of experiments. With animal welfare in mind, only one control group and FUS sti. spleen group were set up; thus, the K1 and K2 group were the same as the H1 and H2 group respectively.

of the tumor, with a smaller effect on tumor suppression. Additionally, the statistical results of liver weight and mice weight showed a decreasing trend in the K2-K4 groups compared to the K1 group (Figure 7E and F). The spleen weight and spleen index also demonstrated that FUS sti. spleen attenuated the symptoms of splenomegaly caused by cancer, as same as in Figure 7G–H.

Statistic FCM results showed that the proportion of NK cells and CD8 T cells was significantly increased in the spleen, blood, tumor, and para-carcinoma tissue of the K2-K4 groups compared with the K1 group, and the proportion of PMN-MDSCs was significantly reduced (Figure 7I–L, Supplementary Figures 29–32). However, no significant difference was found in the number of immune cells among the K2-K4 groups except that NK cells were significantly higher in the K2 group (Figure 7I–L, Supplementary Figures 29–32). In addition, the proportion of Mφ1 and DC1 in four tissues of the K2-K4 groups was significantly increased (Supplementary Figures 29–32). What needs to be highlighted is the inconsistency in the changes in the cell proportion of Mφ2, DC2 or other immune cells in the spleen, blood, tumor, and para-carcinoma tissue (Supplementary Figures 29–32). Our hypothesis was that this phenomenon was mainly attributed to the migration of splenic immune cells to tumor lesions after responding to ultrasonic stimulation and stressing the tumor microenvironment, which was fully demonstrated in our previous work that $CD11b^{+}$ $CD43^{hi}$ $Ly6C^{lo}$ splenocyte-derived Mφ migrate into the lesion in a liver fibrosis model.[82]

Special attention should be paid to the fact that the biological effect of ultrasound on spleen varies in different disease models. As reported by Nunes et al[68] and Liu et al,[83] FUS sti. spleen mainly affects Mφ to inhibit the secretion of inflammatory cytokines in colitis and myocarditis. Also related to RA, CD 4 T cell, CD8 T cell, B cell and myeloid cell populations were significantly changed in response to ultrasound, specifically the CD8 T cells show an evident correlation with FUS sti. spleen based therapy.[84] However, this study fully confirmed that FUS sti. spleen significantly promoted the proliferation of NK cells, CD8 T cells, Mφ1 and DC1 in various tumor models, and reduced PMN-MDSCs, but mainly suppressed cancer progression by stimulating NK cells. Additionally, the biological effects of ultrasound on different types of cells are also varied, including enhancing MC3T3-E1 osteoblasts and hematopoietic stem cell ingrowth, proliferation, and early differentiation,[85,86] inducing neural progenitor cell polarization,[72] promoting proliferation and migration of HaCaT keratinocytes,[73] facilitating the extracellular matrix synthesis of degenerative human nucleus pulposus cells,[87] and motivating the expression of brain-derived neurotrophic factor in astrocyte.[77] However, the difference in biological effects of ultrasound irradiation on various immune cells enriched in the spleen is not yet known and needs to be detailedly studied in the future.

In conclusion, although FUS sti. spleen non-specifically activated spleen immunological function to universally suppress tumor proliferation, it was effective on the early stage of cancer or cancer prevention. Nevertheless, it might be necessary to combine FUS sti. spleen with other treatments in patients with advanced cancer, such as applying FUS qualitatively and quantitatively intervention on the tumor (FUS int. tumor).

FUS Sti. Spleen & FUS Int. Tumor Synergistically Suppress Tumor Proliferation

Previous studies reported that ultrasonic intervention on tumor lesions enhances tumor suppression by promoting the proliferation, activation, and infiltration of immune cells.[88,89] In this study, comparing and discussing FUS sti. spleen and FUS int. tumors – two strategies for immunomodulation to counteract the swelling by interfering from immune organs and tumor foci, respectively – are crucial. Five experimental groups were considered: #1 group, normal mice (mice without any treatment); #2 group, control group of subcutaneous H22 tumor mice; #3 group, FUS sti. spleen on day 0 after H22 cancer cell implantation, and once every two days; #4 group, FUS int. tumor; #5 group, FUS sti. spleen and FUS int. tumor synergistic treatment. At the experimental endpoint (day 29), animals underwent terminal anesthesia followed by comprehensive tissue harvesting for other experimental analyses (eg, FCM). According to pre-experiments and our previous results,[90] FUS int. tumor was performed every 4 days from day 9 after the subcutaneous inoculation of H22 cancer cells (Figure 8A), and the ultrasonic parameters were set to 3.3 MPa, 1%, 20s to achieve controlled disruption of tumor's extracellular matrix barrier and tumor microenvironment, thereby enhancing immunomodulatory effects without excessively compromising tissue architecture or inducing cellular necrosis.

The results of #3 vs #2 group again confirmed the ability and application prospect of FUS sti. spleen in suppressing tumor proliferation (Figure 8B–D). Moreover, FUS int. tumor showed an effective tumor suppression (#4 vs #2 group; Figure 8B–D), but it did not show any significant difference as compared with the #3 group (Figure 8B–D). It was noteworthy that FUS sti. spleen and FUS int. tumor synergistically induced the best tumor suppression (Figure 8B–D). In addition, FUS sti. spleen and FUS int. tumor synergistically or either alone reduced the mice weight (Figure 8E), but the combined application significantly exacerbated splenomegaly (Figure 8F and G).

https://doi.org/10.2147/ITT.S534444

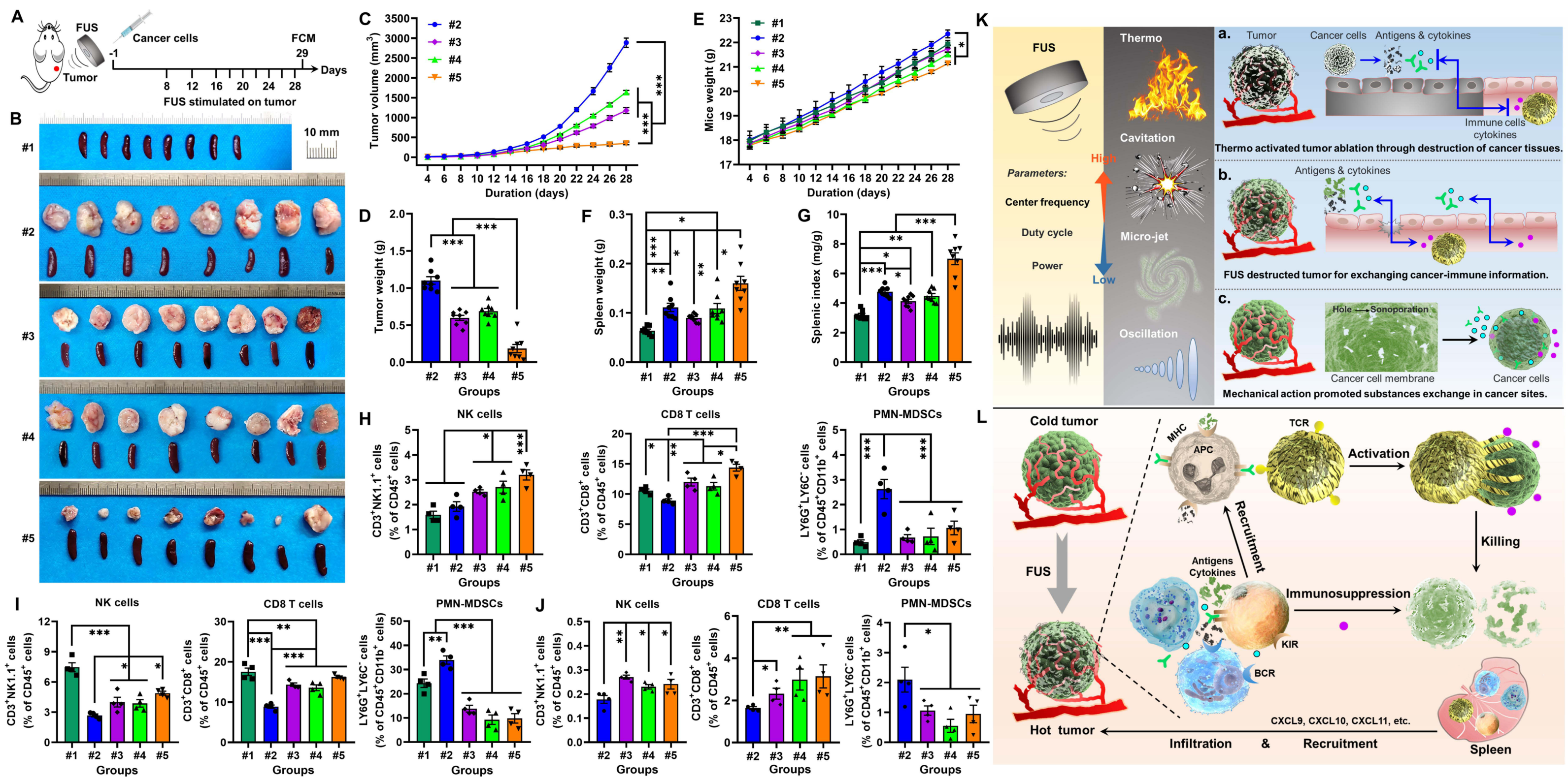

Figure 8 FUS sti. spleen and FUS int. tumor synergistically or individually suppressed the proliferation of the subcutaneous H22 HCC tumor. (**A**) experimental flow diagram of FUS int. tumor every four days started on day 8 after H22 cancer cell implantation. (**B**) image of spleen and tumor. (**C**) tumor volume. (**D**) tumor weight. (**E**) curve of mice weight. (**F**) spleen weight. (**G**) spleen index, the ratio of spleen weight to mouse weight. (n = 8; * p ≤ 0.05; **p ≤ 0.01; ***p ≤ 0.001; mean ± SEM). (**H–J)** FCM results of NK cells, CD8 T cells and PMN-MDSCs in the spleen, blood, and tumor, respectively. (n = 4; * p ≤ 0.05; **p ≤ 0.01; ***p ≤ 0.001; mean ± SEM). (**K** and **L)** schematic illustration of the mechanism during FUS int. tumor to enhance anticancer immune response of FUS sti. spleen. #1, normal mice group; #2, control group of subcutaneous H22 tumor mice; #3, FUS sti. spleen on the second day after H22 cancer cell implantation; #4, FUS int. tumor; #5, FUS sti. spleen and FUS int. tumor synergistic effect.

FCM results revealed that the proportion of NK cells and CD8 T cells in the spleen, blood and tumor was significantly and synergistically increased compared to the effect of each of the two taken individually (Figure 8H–J). The comparison of the #3-#5 groups revealed that the number of NK cells and CD8 T cells in the spleen and blood was significantly higher after H22 tumor-bearing mice were subjected to the synergistic effect of FUS sti. spleen and FUS int. tumor compared to the effect of each of the two taken individually (Figure 8H and I). However, such a trend in the number of immune cells was not present in tumor tissues, which was mainly attributed to the fact that FUS int. tumor not only disrupted the structure of tumor stromal barrier and cancer cells, but also killed immune cells. Additionally, FUS sti. spleen, FUS int. tumor or both synergistically significantly increased the proportion of Mφ1 or DC1 in the spleen, blood, and tumor (Supplementary Figures 33–35). However, consistent with the FCM results in Table 2, FUS sti. spleen had no significant consistent effect on CD4 T cells or their subtype in the spleen, blood, and tumor from subcutaneous H22 tumor-bearing mice.

FUS has been gradually developed into a clinical strategy approach for targeted tumor disruption through thermal mechanisms.[91–93] In essence, FUS at high intensity generated focal temperatures exceeding 60 °C that instantaneously caused coagulative necrosis of the target soft tissue (Figure 8K).[94,95] In contrast, non-thermomechanical disruption may have a more relevant role in low intensity FUS ablation, particularly in terms of immunomodulatory effects. As opposite to thermal ablation causing protein coagulation necrosis, the mechanical disruption of FUS int. tumor converts immunologically "cold" (poorly infiltrated) tumors into immunologically "hot" (well-infiltrated) ones by damaging cancer cells to release antigens, collapsing the tumor matrix barrier to enhance antigens captured by immune cells, and especially intensifying the infiltration of immune cells and cytokines into the tumor lesions, which strengthened the immunotherapeutic responses to cancer (Figure 8K and L).[88,96] Although FUS int. tumor alone exerted an anti-tumor effect, to a certain extent, the tumor matrix damage would increase the risk of cancer cell spread and metastasis.[97] However, in this study, the synergistic use of FUS sti. spleen and FUS int. tumor was much more effective, since tumor disruption by FUS provided an antigen source for activating splenic immune cells during the process of FUS sti. spleen to suppress tumor proliferation (Figure 8L).

Discussion

The comparison of tumor inhibition and spleen injury under different ultrasonic parameters of FUS sti. spleen revealed that the spleen (or splenic cells) had significant ultrasound dose dependence and tolerance. This was also reported in previous studies; for example, Liu et al[83] successfully screened an effective ultrasonic parameter of 0.35 MPa with a 1s on /5s off duty cycle to significantly alleviate autoimmune myocarditis, and regulate the proportion and function of Tregs and Mφ by activating CAP. Besides, Cotero et al[23] discovered that non-invasive splenic ultrasound stimulation at 0.83 MPa effectively alleviates the severity of arthritis and reduces cytokine response to endotoxin through CAP modulation based on $CD4^+$ T cells. However, according to a summary of studies (Supplementary Table 3), although splenic ultrasound stimulation can effectively suppress various inflammatory diseases, the ultrasonic parameters applied for spleen stimulation are extremely variable. Some studies only referred to the ultrasonic parameters mentioned in previous reports but lacked screening and optimization; for example, Hu et al[84] and Morton et al[98] used the parameters of 0.35 MPa and 1-s on/5-s off reported by Zachs et al[30] for splenic immunomodulation to treat inflammatory diseases. However, in practical applications, different ultrasound platforms lead to significant differences in ultrasonic focal region. More importantly, although some studies proved that the mechanism of splenic ultrasound stimulation for inflammatory disease therapy is based on CAP activation,[23,29,69] some other studies demonstrated the direct action of ultrasound on splenic immune cells.[30,84] Therefore, the dependence, specificity, and mechanism of spleen response to ultrasonic stimulation is also different, which may be one of the reasons for the different ultrasonic parameters applied in the above studies. This study also demonstrated that FUS sti. spleen to modulate immune function for tumor suppression was not mainly by activating CAP but depended on the direct stimulation of the proliferation and activation of NK cells, as well as the biological effects of ultrasonic stimulation on CD8 T cells, Mφ, DCs and MDSCs.

At present, there is a lack of studies on splenic ultrasound stimulation to regulate immunotherapy for various diseases; thus, ultrasonic parameters are not objectively consistent, which seriously restricts the translational progress of clinical application. Even if the ultrasonic parameters were screened and optimized in this study, there are still some shortcomings. For example, when the ultrasonic intensity is less than 2.3 MPa, the effect of a longer duration of ultrasound irradiation on splenic immune modulation for tumor suppression needs to be further studied. Fortunately, there are two studies of splenic ultrasound stimulation for immunotherapy on inflammatory diseases registered in http://www.clinicaltrials.gov (NCT03690466, and NCT03548116), but their clinical results are not yet officially published. We look forward to their positive news, and expect that FUS sti. spleen can be widely employed in clinical treatment to alleviate patient suffering.

Conclusion

Combined under optimized ultrasound parameters (2.3 MPa, 1%, and 20s), FUS sti. spleen has been demonstrated to directly activate splenic immune cells, particularly NK cells and $CD8^{+}$ T lymphocytes, through altering calcium-dependent signaling but without significant involvement of cholinergic neuroimmune modulation, thereby effectively suppressing early-to-intermediate stage malignancies. With perspective, concurrent FUS sti. spleen and FUS int. tumor significantly achieve superior therapeutic outcomes, indicating substantial clinical translation potential that warrants further validation through animal and clinical trials.

Abbreviations

IRI, ischemia-reperfusion injury; VNS, vagus nerve stimulation; α7nAChR, α7 nicotinic acetylcholine receptors; FUS, focused ultrasound; DC, dendritic cell; NK, natural killer; MDSC, myeloid-derived suppressor cell; M-MDSC, monocytic myeloid-derived suppressor cell; PMN-MDSC, polymorphonucler myeloid-derived suppressor cell; Mφ, macrophage; Treg, regulatory T cells; FCM, flow cytometry; HCC, hepatocellular carcinoma; TNF-α, tumor necrosis factor α; CAP, cholinergic anti-inflammatory pathway; NE, norepinephrine; ACh, acetylcholine; IgA, immunoglobulin A.

Data Sharing Statement

Raw and analyzed sequencing data in this study have been deposited in the NCBI's Gene Expression Omnibus (under series accession code GSE267237 and GSE267445).

Ethical Approval

All animal experiments were performed in accordance with the institutional guidelines and approved by the Animal Experimentation Ethics Committee of Xi'an Jiaotong University. Additionally, all methodological protocols were designed and reported in accordance with the ARRIVE guidelines for the welfare of the laboratory animals.

Acknowledgments

We thank Hongwei Tian, Gaixia He and Haiyan Chen for providing technical support in preparation of animal models. We thank Pro. Pengfei Liu, Pro. Guangyao Kong, Pro. Yujin Zong, Pro. Shemin Lv and Pro. Tielin Yang for their careful guidance on the design of experimental scheme. In addition, Wei Dong thanks the care and support from Yinggang Zhang, Shoufei Qu, Yameng Wei, Shaoying Zhang, Pro. Jun Li and Pro. Fanpu Ji in the past 2 years.

We would like to thank MogoEdit (https://www.mogoedit.com) for its English editing during the preparation of this manuscript. And we sincerely thank Shanghai OE Biotech Co., LTD (https://www.oebiotech.com/) for the RNA sequencing and data analysis.

This paper has been uploaded to ResearchSquare and bioRxiv as a preprint: https://www.researchsquare.com/article/rs-4639146/v1; https://www.biorxiv.org/content/10.1101/2025.03.31.646454v1.

Funding

This work was supported by the National Natural Science Foundation of China (No. 12204370), the Innovation Ability Supporting Program of Shaanxi Province (No. 2023WGZJ-ZD-09), and the Basic-Clinical Integration Innovation Project of Xi 'an Jiaotong University (No. YXJLRH2022092).

Disclosure

The authors declare that they have no competing interests in this work.

References

1. Verlinden TJM, van Dijk P, Hikspoors J, Herrler A, Lamers WH, Köhler SE. Innervation of the human spleen: a complete hilum-embedding approach. *Brain Behav Immun*. 2019;77:92–100. doi:10.1016/j.bbi.2018.12.009
2. Hu D, Al-Shalan HAM, Shi Z, et al. Distribution of nerve fibers and nerve-immune cell association in mouse spleen revealed by immunofluorescent staining. *Scientific Reports*. 2020;10(1):9850. doi:10.1038/s41598-020-66619-0
3. Anagnostou VK, Doussis-Anagnostopoulou I, Tiniakos DG, et al. Ontogeny of intrinsic innervation in the human thymus and spleen. *J Histochem Cytochem*. 2007;55(8):813–820. doi:10.1369/jhc.6A7168.2007
4. Elenkov IJ, Vizi ES. Presynaptic modulation of release of noradrenaline from the sympathetic nerve terminals in the rat spleen. *Neuropharmacology.* 1991;30(12a):1319–1324. doi:10.1016/0028-3908(91)90029-B
5. Sudo A. Decrease in Adrenaline content of various organs of the rat after 6-hydroxydopamine. *Eur J Pharmacol*. 1985;114(1):79–83. doi:10.1016/0014-2999(85)90524-2
6. Pavlov VA, Tracey KJ. The vagus nerve and the inflammatory reflex--linking immunity and metabolism. *Nat Rev Endocrinol*. 2012;8(12):743–754. doi:10.1038/nrendo.2012.189
7. Tracey KJ. Reflex control of immunity. *Nat Rev Immunol*. 2009;9(6):418–428. doi:10.1038/nri2566
8. Tracey KJ. Reflexes in Immunity. *Cell*. 2016;164(3):343–344. doi:10.1016/j.cell.2016.01.018
9. Borovikova LV, Ivanova S, Zhang M, et al. Vagus nerve stimulation attenuates the systemic inflammatory response to endotoxin. *Nature*. 2000;405(6785):458–462. doi:10.1038/35013070
10. Bai A, Guo Y, Lu N. The effect of the cholinergic anti-inflammatory pathway on experimental colitis. *Scand J Immunol*. 2007;66(5):538–545. doi:10.1111/j.1365-3083.2007.02011.x
11. Munyaka P, Rabbi MF, Pavlov VA, Tracey KJ, Khafipour E, Ghia JE. Central muscarinic cholinergic activation alters interaction between splenic dendritic cell and CD4+CD25- T cells in experimental colitis. *PLoS One*. 2014;9(10):e109272. doi:10.1371/journal.pone.0109272
12. Ji H, Rabbi MF, Labis B, Pavlov VA, Tracey KJ, Ghia JE. Central cholinergic activation of a vagus nerve-to-spleen circuit alleviates experimental colitis. *Mucosal Immunol*. 2014;7(2):335–347. doi:10.1038/mi.2013.52
13. Bonaz B, Sinniger V, Pellissier S. Vagus nerve stimulation: a new promising therapeutic tool in inflammatory bowel disease. *J Intern Med*. 2017;282(1):46–63. doi:10.1111/joim.12611
14. Inoue T, Abe C, Sung SS, et al. Vagus nerve stimulation mediates protection from kidney ischemia-reperfusion injury through α7nAChR+ splenocytes. *J Clin Invest*. 2016;126(5):1939–1952. doi:10.1172/JCI83658
15. Koopman FA, Schuurman PR, Vervoordeldonk MJ, Tak PP. Vagus nerve stimulation: a new bioelectronics approach to treat rheumatoid arthritis? *Best Pract Res Clin Rheumatol*. 2014;28(4):625–635. doi:10.1016/j.berh.2014.10.015
16. Koopman FA, Chavan SS, Miljko S, et al. Vagus nerve stimulation inhibits cytokine production and attenuates disease severity in rheumatoid arthritis. *Proc Natl Acad Sci U S A*. 2016;113(29):8284–8289. doi:10.1073/pnas.1605635113
17. Meregnani J, Clarençon D, Vivier M, et al. Anti-inflammatory effect of vagus nerve stimulation in a rat model of inflammatory bowel disease. *Auton Neurosci*. 2011;160(1–2):82–89. doi:10.1016/j.autneu.2010.10.007
18. Zhang Z, Yu Q, Zhang X, et al. Electroacupuncture regulates inflammatory cytokines by activating the vagus nerve to enhance antitumor immunity in mice with breast tumors. *Life Sci*. 2021;272:119259. doi:10.1016/j.lfs.2021.119259
19. Li QW, Yu MW, Yang GW, et al. Effect of acupuncture in prevention and treatment of chemotherapy-induced nausea and vomiting in patients with advanced cancer: study protocol for a randomized controlled trial. *Trials*. 2017;18(1):185. doi:10.1186/s13063-017-1927-2
20. Li QW, Yu MW, Wang XM, et al. Efficacy of acupuncture in the prevention and treatment of chemotherapy-induced nausea and vomiting in patients with advanced cancer: a multi-center, single-blind, randomized, sham-controlled clinical research. *Chin Med*. 2020;15:57. doi:10.1186/s13020-020-00333-x
21. Rush AJ, Marangell LB, Sackeim HA, et al. Vagus nerve stimulation for treatment-resistant depression: a randomized, controlled acute phase trial. *Biol Psychiatry.* 2005;58(5):347–354. doi:10.1016/j.biopsych.2005.05.025
22. Rush AJ, Sackeim HA, Marangell LB, et al. Effects of 12 months of vagus nerve stimulation in treatment-resistant depression: a naturalistic study. *Biol Psychiatry.* 2005;58(5):355–363. doi:10.1016/j.biopsych.2005.05.024
23. Cotero V, Fan Y, Tsaava T, et al. Noninvasive sub-organ ultrasound stimulation for targeted neuromodulation. *Nature Communications*. 2019;10(1):952. doi:10.1038/s41467-019-08750-9
24. Olofsson PS, Tracey KJ. Bioelectronic medicine: technology targeting molecular mechanisms for therapy. *J Intern Med*. 2017;282(1):3–4. doi:10.1111/joim.12624
25. Bassi GS, Dias DPM, Franchin M, et al. Modulation of experimental arthritis by vagal sensory and central brain stimulation. *Brain Behav Immun*. 2017;64:330–343. doi:10.1016/j.bbi.2017.04.003
26. Martelli D, McKinley MJ, McAllen RM. The cholinergic anti-inflammatory pathway: a critical review. *Auton Neurosci*. 2014;182:65–69. doi:10.1016/j.autneu.2013.12.007
27. Mei H, Irazoqui PP. Miniaturizing wireless implants. *Nat Biotechnol*. 2014;32(10):1008–1010. doi:10.1038/nbt.3038
28. Fattahi P, Yang G, Kim G, Abidian MR. A review of organic and inorganic biomaterials for neural interfaces. *Adv Mater*. 2014;26(12):1846–1885. doi:10.1002/adma.201304496
29. Gigliotti JC, Huang L, Ye H, et al. Ultrasound prevents renal ischemia-reperfusion injury by stimulating the splenic cholinergic anti-inflammatory pathway. *J Am Soc Nephrol*. 2013;24(9):1451–1460. doi:10.1681/ASN.2013010084
30. Zachs DP, Offutt SJ, Graham RS, et al. Noninvasive ultrasound stimulation of the spleen to treat inflammatory arthritis. *Nat Commun*. 2019;10(1):951. doi:10.1038/s41467-019-08721-0
31. Dong W, Li Y, Fei Q, et al. Targeted spleen modulation: a novel strategy for next-generation disease immunotherapy. *Theranostics*. 2025;15(10):4416–4445. doi:10.7150/thno.111116

32. Yahata K, Kanno H, Ozawa H, et al. Low-energy extracorporeal shock wave therapy for promotion of vascular endothelial growth factor expression and angiogenesis and improvement of locomotor and sensory functions after spinal cord injury. *J Neurosurg Spine*. 2016;25(6):745–755. doi:10.3171/2016.4.SPINE15923
33. Ito K, Fukumoto Y, Shimokawa H. Extracorporeal shock wave therapy for ischemic cardiovascular disorders. *Am J Cardiovasc Drugs*. 2011;11 (5):295–302. doi:10.2165/11592760-000000000-00000
34. Vezeridis PS, Semeins CM, Chen Q, Klein-Nulend J. Osteocytes subjected to pulsating fluid flow regulate osteoblast proliferation and differentiation. *Biochem Biophys Res Commun*. 2006;348(3):1082–1088. doi:10.1016/j.bbrc.2006.07.146
35. Fung CH, Cheung WH, Pounder NM, Harrison A, Leung KS. Osteocytes exposed to far field of therapeutic ultrasound promotes osteogenic cellular activities in pre-osteoblasts through soluble factors. *Ultrasonics*. 2014;54(5):1358–1365. doi:10.1016/j.ultras.2014.02.003
36. Shin VY, Jin HC, Ng EK, et al. Nicotine and 4-(methylnitrosamino)-1-(3-pyridyl)-1-butanone induce cyclooxygenase-2 activity in human gastric cancer cells: involvement of nicotinic acetylcholine receptor (nAChR) and beta-adrenergic receptor signaling pathways. *Toxicol Appl Pharmacol*. 2008;233(2):254–261. doi:10.1016/j.taap.2008.08.012
37. Maccari S, Profumo E, Saso L, Marano G, Buttari B. Propranolol promotes monocyte-to-macrophage differentiation and enhances macrophage anti-inflammatory and antioxidant activities by NRF2 activation. *Int J Mol Sci*. 2024;25(7):3683. doi:10.3390/ijms25073683
38. Chai GS, Wu JJ, Gong J, et al. Activation of β2-adrenergic receptor ameliorates amyloid-β-induced mitophagy defects and tau pathology in mice. *Neuroscience*. 2022;505:34–50. doi:10.1016/j.neuroscience.2022.09.020
39. Shionoya Y, Sunada K, Shigeno K, Nakada A, Honda M, Nakamura T. Can nerve regeneration on an artificial nerve conduit be enhanced by ethanol-induced cervical sympathetic ganglion block? *PLoS One*. 2017;12(12):e0189297. doi:10.1371/journal.pone.0189297
40. Liu M, Ni H, Tao J, Xie K. Lumbar sympathetic nerve modulation using absolute ethanol for the treatment of primary lower-extremity hyperhidrosis: a dose-effect pilot study. *Med Sci Monit*. 2021;27:e928209. doi:10.12659/MSM.928209
41. Shionoya Y, Sunada K, Tsujimoto G, Shigeno K, Nakamura T. Ethanol-induced cervical sympathetic ganglion block applications for promoting canine inferior alveolar nerve regeneration using an artificial nerve. *J Vis Exp*. 2018;141.
42. Lu X, Li B, Liu S, Zhu J, Li J. The dose and volume-response relationship of an ethanol-induced tibial nerve block in a rabbit model. *Am J Phys Med Rehabil*. 2014;93(2):138–145. doi:10.1097/PHM.0b013e3182a92b57
43. Pham-Marcou TA, Gentili M, Asehnoune K, Fletcher D, Mazoit JX. Effect of neurolytic nerve block on systemic carrageenan-induced inflammatory response in mice. *Br J Anaesth*. 2005;95(2):243–246. doi:10.1093/bja/aei150
44. Zhang X, Lei B, Yuan Y, et al. Brain control of humoral immune responses amenable to behavioural modulation. *Nature*. 2020;581(7807):204–208. doi:10.1038/s41586-020-2235-7
45. Tuomela K, Ambrose AR, Davis DM. Escaping death: how cancer cells and infected cells resist cell-mediated cytotoxicity. *Front Immunol*. 2022;13:867098. doi:10.3389/fimmu.2022.867098
46. Kuerten S, Nowacki TM, Kleen TO, Asaad RJ, Lehmann PV, Tary-Lehmann M. Dissociated production of perforin, granzyme B, and IFN-gamma by HIV-specific CD8(+) cells in HIV infection. *AIDS Res Hum Retroviruses*. 2008;24(1):62–71. doi:10.1089/aid.2007.0125
47. Hodge G, Barnawi J, Jurisevic C, et al. Lung cancer is associated with decreased expression of perforin, granzyme B and interferon (IFN)-γ by infiltrating lung tissue T cells, natural killer (NK) T-like and NK cells. *Clin Exp Immunol*. 2014;178(1):79–85. doi:10.1111/cei.12392
48. Chen S, Jiao J, Jiang D, et al. T-box transcription factor Brachyury in lung cancer cells inhibits macrophage infiltration by suppressing CCL2 and CCL4 chemokines. *Tumour Biol*. 2015;36(8):5881–5890. doi:10.1007/s13277-015-3260-2
49. Ottaviani C, Nasorri F, Bedini C, de Pità O, Girolomoni G, Cavani A. CD56brightCD16(-) NK cells accumulate in psoriatic skin in response to CXCL10 and CCL5 and exacerbate skin inflammation. *Eur J Immunol*. 2006;36(1):118–128. doi:10.1002/eji.200535243
50. Ghafouri-Fard S, Shahir M, Taheri M, Salimi A. A review on the role of chemokines in the pathogenesis of systemic lupus erythematosus. *Cytokine*. 2021;146:155640. doi:10.1016/j.cyto.2021.155640
51. Janssens R, Struyf S, Proost P. The unique structural and functional features of CXCL12. *Cell Mol Immunol*. 2018;15(4):299–311. doi:10.1038/cmi.2017.107
52. Janssens R, Struyf S, Proost P. Pathological roles of the homeostatic chemokine CXCL12. *Cytokine Growth Factor Rev*. 2018;44:51–68. doi:10.1016/j.cytogfr.2018.10.004
53. Gouwy M, Schiraldi M, Struyf S, Van Damme J, Uguccioni M. Possible mechanisms involved in chemokine synergy fine tuning the inflammatory response. *Immunol Lett*. 2012;145(1–2):10–14. doi:10.1016/j.imlet.2012.04.005
54. Zhou W, Guo S, Liu M, Burow ME, Wang G. Targeting CXCL12/CXCR4 axis in tumor immunotherapy. *Curr Med Chem*. 2019;26(17):3026–3041. doi:10.2174/0929867324666170830111531
55. Yang Y, Li J, Lei W, et al. CXCL12-CXCR4/CXCR7 axis in cancer: from mechanisms to clinical applications. *Int J Biol Sci*. 2023;19 (11):3341–3359. doi:10.7150/ijbs.82317
56. Urdinguio RG, Fernandez AF, Moncada-Pazos A, et al. Immune-dependent and independent antitumor activity of GM-CSF aberrantly expressed by mouse and human colorectal tumors. *Cancer Res*. 2013;73(1):395–405. doi:10.1158/0008-5472.CAN-12-0806
57. Bretscher V, Andreutti D, Neuville P, et al. GM-CSF expression by tumor cells correlates with aggressivity and with stroma reaction formation. *J Submicrosc Cytol Pathol*. 2000;32(4):525–533.
58. Hong IS. Stimulatory versus suppressive effects of GM-CSF on tumor progression in multiple cancer types. *Exp Mol Med*. 2016;48(7):e242. doi:10.1038/emm.2016.64
59. Thorn M, Guha P, Cunetta M, et al. Tumor-associated GM-CSF overexpression induces immunoinhibitory molecules via STAT3 in myeloid-suppressor cells infiltrating liver metastases. *Cancer Gene Ther*. 2016;23(6):188–198. doi:10.1038/cgt.2016.19
60. Sweet MJ, Hume DA. CSF-1 as a regulator of macrophage activation and immune responses. *Arch Immunol Ther Exp*. 2003;51(3):169–177.
61. Hume DA, MacDonald KP. Therapeutic applications of macrophage colony-stimulating factor-1 (CSF-1) and antagonists of CSF-1 receptor (CSF-1R) signaling. *Blood*. 2012;119(8):1810–1820. doi:10.1182/blood-2011-09-379214
62. Malkova AM, Gubal AR, Petrova AL, et al. Pathogenetic role and clinical significance of interleukin-1β in cancer. *Immunology*. 2023;168 (2):203–216. doi:10.1111/imm.13486
63. Zhou J, Tulotta C, Ottewell PD. IL-1β in breast cancer bone metastasis. *Expert Rev Mol Med*. 2022;24:e11. doi:10.1017/erm.2022.4
64. Rébé C, Ghiringhelli F. Interleukin-1β and Cancer. *Cancers*. 2020;12(7):1791. doi:10.3390/cancers12071791
65. Mizui M. Natural and modified IL-2 for the treatment of cancer and autoimmune diseases. *Clin Immunol*. 2019;206:63–70. doi:10.1016/j.clim.2018.11.002

66. Corrêa LH, Corrêa R, Farinasso CM, de Sant'Ana Dourado LP, Magalhães KG. Adipocytes and macrophages interplay in the orchestration of tumor microenvironment: new implications in cancer progression. *Front Immunol*. 2017;8:1129. doi:10.3389/fimmu.2017.01129
67. Becker Y. Molecular immunological approaches to biotherapy of human cancers--a review, hypothesis and implications. *Anticancer Res*. 2006;26 (2a):1113–1134.
68. Nunes NS, Chandran P, Sundby M, et al. Therapeutic ultrasound attenuates DSS-induced colitis through the cholinergic anti-inflammatory pathway. *EBioMedicine*. 2019;45:495–510. doi:10.1016/j.ebiom.2019.06.033
69. Ahmed U, Graf JF, Daytz A, et al. Ultrasound neuromodulation of the spleen has time-dependent anti-inflammatory effect in a pneumonia model. *Front Immunol*. 2022;13:892086. doi:10.3389/fimmu.2022.892086
70. Li BH, Jiang W, Zhang S, et al. The spleen contributes to the increase in PMN-MDSCs in orthotopic H22 hepatoma mice. *Mol Immunol*. 2020;125:95–103. doi:10.1016/j.molimm.2020.07.002
71. Li Y, Wang X, Cheng C, Jiang S, Ma T, Xu L. Absence of MHC class II molecules promotes natural killer cells activation in mice. *Int Immunopharmacol*. 2020;88:106888. doi:10.1016/j.intimp.2020.106888
72. Lee IC, Wu HJ, Liu HL. Dual-frequency ultrasound induces neural stem/progenitor cell differentiation and growth factor utilization by enhancing stable cavitation. *ACS Chem Neurosci*. 2019;10(3):1452–1461. doi:10.1021/acschemneuro.8b00483
73. Leng X, Shang J, Gao D, Wu J. Low-intensity pulsed ultrasound promotes proliferation and migration of HaCaT keratinocytes through the PI3K/ AKT and JNK pathways. *Braz J Med Biol Res*. 2018;51(12):e7862. doi:10.1590/1414-431x20187862
74. Xing J, Singh S, Zhao Y, et al. Increasing vaccine production using pulsed ultrasound waves. *PLoS One*. 2017;12(11):e0187048. doi:10.1371/ journal.pone.0187048
75. Komiyama K, Crago SS, Itoh K, Moro I, Mestecky J. Inhibition of natural killer cell activity by IgA. *Cell Immunol*. 1986;101(1):143–155. doi:10.1016/0008-8749(86)90193-0
76. Moţa G, Galatiuc C, Popescu I, Hirt M, Cialâcu V, Sulică A. IgA monoclonal and polyclonal proteins as regulatory factors of the NK cytotoxic activity. *Rom J Virol*. 1999;50(1–4):17–31.
77. Liu SH, Lai YL, Chen BL, Yang FY. Ultrasound enhances the expression of brain-derived neurotrophic factor in astrocyte through activation of TrkB-Akt and calcium-CaMK signaling pathways. *Cereb Cortex*. 2017;27(6):3152–3160. doi:10.1093/cercor/bhw169
78. Burks SR, Lorsung RM, Nagle ME, Tu TW, Frank JA. Focused ultrasound activates voltage-gated calcium channels through depolarizing TRPC1 sodium currents in kidney and skeletal muscle. *Theranostics*. 2019;9(19):5517–5531. doi:10.7150/thno.33876
79. Yoon CW, Lee NS, Koo KM, et al. Investigation of ultrasound-mediated intracellular Ca(2+) oscillations in HIT-T15 pancreatic β-cell line. *Cells*. 2020;9(5). doi:10.3390/cells9051129
80. Dautova Y, Kapustin AN, Pappert K, et al. Calcium phosphate particles stimulate interleukin-1β release from human vascular smooth muscle cells: a role for spleen tyrosine kinase and exosome release. *J Mol Cell Cardiol*. 2018;115:82–93. doi:10.1016/j.yjmcc.2017.12.007
81. de Water R, Leenen PJ, Noordermeer C, et al. Cytokine production induced by binding and processing of calcium oxalate crystals in cultured macrophages. *Am J Kidney Dis*. 2001;38(2):331–338. doi:10.1053/ajkd.2001.26098
82. Zhang S, Wan D, Zhu M, et al. CD11b + CD43 hi Ly6C lo splenocyte-derived macrophages exacerbate liver fibrosis via spleen-liver axis. *Hepatology*. 2023;77(5):1612–1629. doi:10.1002/hep.32782
83. Liu T, Fu Y, Shi J, et al. Noninvasive ultrasound stimulation to treat myocarditis through splenic neuro-immune regulation. *J Neuroinflammation*. 2023;20(1):94. doi:10.1186/s12974-023-02773-2
84. Hu X, Li F, Zeng J, et al. Noninvasive low-frequency pulsed focused ultrasound therapy for rheumatoid arthritis in mice. *Research*. 2022;2022:0013. doi:10.34133/research.0013
85. Wu L, Lin L, Qin YX. Enhancement of cell ingrowth, proliferation, and early differentiation in a three-dimensional silicon carbide scaffold using low-intensity pulsed ultrasound. *Tissue Eng Part A*. 2015;21(1–2):53–61. doi:10.1089/ten.tea.2013.0597
86. Xu P, Gul-Uludag H, Ang WT, et al. Low-intensity pulsed ultrasound-mediated stimulation of hematopoietic stem/progenitor cell viability, proliferation and differentiation in vitro. *Biotechnol Lett*. 2012;34(10):1965–1973. doi:10.1007/s10529-012-0984-6
87. Zhang X, Hu Z, Hao J, Shen J. Low intensity pulsed ultrasound promotes the extracellular matrix synthesis of degenerative human nucleus pulposus cells through FAK/PI3K/Akt pathway. *Spine*. 2016;41(5):E248–54. doi:10.1097/BRS.0000000000001220
88. Qu S, Worlikar T, Felsted AE, et al. Non-thermal histotripsy tumor ablation promotes abscopal immune responses that enhance cancer immunotherapy. *J Immunother Cancer*. 2020;8(1). doi:10.1136/jitc-2019-000200
89. Mauri G, Nicosia L, Xu Z, et al. Focused ultrasound: tumour ablation and its potential to enhance immunological therapy to cancer. *Br J Radiol*. 2018;91(1083):20170641. doi:10.1259/bjr.20170641
90. Dong W, Wu P, Zhou D, et al. Ultrasound-mediated gene therapy of hepatocellular carcinoma using pre-microRNA plasmid-loaded nanodroplets. *Ultrasound Med Biol*. 2020;46(1):90–107. doi:10.1016/j.ultrasmedbio.2019.09.016
91. Hoogenboom M, Eikelenboom D, den Brok MH, Heerschap A, Fütterer JJ, Adema GJ. Mechanical high-intensity focused ultrasound destruction of soft tissue: working mechanisms and physiologic effects. *Ultrasound Med Biol*. 2015;41(6):1500–1517. doi:10.1016/j.ultrasmedbio.2015.02.006
92. Izadifar Z, Babyn P, Chapman D. Mechanical and biological effects of ultrasound: a review of present knowledge. *Ultrasound Med Biol*. 2017;43 (6):1085–1104. doi:10.1016/j.ultrasmedbio.2017.01.023
93. Cheung TT, Chu FS, Jenkins CR, et al. Tolerance of high-intensity focused ultrasound ablation in patients with hepatocellular carcinoma. *World J Surg*. 2012;36(10):2420–2427. doi:10.1007/s00268-012-1660-7
94. Hoogenboom M, Eikelenboom D, den Brok MH, et al. In vivo MR guided boiling histotripsy in a mouse tumor model evaluated by MRI and histopathology. *NMR Biomed*. 2016;29(6):721–731. doi:10.1002/nbm.3520
95. Zhou YF. High intensity focused ultrasound in clinical tumor ablation. *World J Clin Oncol*. 2011;2(1):8–27. doi:10.5306/wjco.v2.i1.8
96. Sheybani ND, Price RJ. Perspectives on recent progress in focused ultrasound immunotherapy. *Theranostics*. 2019;9(25):7749–7758. doi:10.7150/ thno.37131
97. Curley CT, Sheybani ND, Bullock TN, Price RJ. Focused ultrasound immunotherapy for central nervous system pathologies: challenges and opportunities. *Theranostics*. 2017;7(15):3608–3623. doi:10.7150/thno.21225
98. Morton C, Cotero V, Ashe J, Ginty F, Puleo C. Accelerating cutaneous healing in a rodent model of type II diabetes utilizing non-invasive focused ultrasound targeted at the spleen. *Front Neurosci*. 2022;16:1039960.

ImmunoTargets and Therapy

Dovepress
Taylor & Francis Group

Publish your work in this journal

ImmunoTargets and Therapy is an international, peer-reviewed open access journal focusing on the immunological basis of diseases, potential targets for immune based therapy and treatment protocols employed to improve patient management. Basic immunology and physiology of the immune system in health, and disease will be also covered. In addition, the journal will focus on the impact of management programs and new therapeutic agents and protocols on patient perspectives such as quality of life, adherence and satisfaction. The manuscript management system is completely online and includes a very quick and fair peer-review system, which is all easy to use. Visit http://www.dovepress.com/testimonials.php to read real quotes from published authors.

Submit your manuscript here: http://www.dovepress.com/immunotargets-and-therapy-journal